

The magnification factor accounts for the greater hypometria and imprecision of larger saccades: Evidence from a parametric human-behavioral study

Françoise Vitu

Laboratoire de Psychologie Cognitive, CNRS,
Aix-Marseille Université, Marseille, France



Soazig Casteau

Laboratoire de Psychologie Cognitive, CNRS,
Aix-Marseille Université, Marseille, France



Hossein Adeli

Department of Psychology, Stony Brook University,
Stony Brook, NY, USA



Gregory J. Zelinsky

Departments of Psychology and Computer Science,
Stony Brook University,
Stony Brook, NY, USA



Eric Castet

Laboratoire de Psychologie Cognitive, CNRS,
Aix-Marseille Université, Marseille, France



Saccades quite systematically undershoot a peripheral visual target by about 10% of its eccentricity while becoming more variable, mainly in amplitude, as the target becomes more peripheral. This undershoot phenomenon has been interpreted as the strategic adjustment of saccadic gain downstream of the superior colliculus (SC), where saccades are programmed. Here, we investigated whether the eccentricity-related increase in saccades' hypometria and imprecision might not instead result from overrepresentation of space closer to the fovea in the SC and visual-cortical areas. To test this magnification-factor (MF) hypothesis, we analyzed four parametric eye-movement data sets, collected while humans made saccades to single eccentric stimuli. We first established that the undershoot phenomenon generalizes to ordinary saccade amplitudes (0.5° – 15°) and directions (0° – 90°) and that landing-position distributions become not only increasingly elongated but also more skewed toward the fovea as target eccentricity increases. Moreover, we confirmed the MF hypothesis by showing (a) that the linear eccentricity-related increase in undershoot error and negative skewness canceled out when landing positions were log-scaled according to the MF in monkeys' SC and (b) that the spread, proportional to eccentricity outside an extended, 5° , foveal region,

became circular and invariant in size in SC space. Yet the eccentricity-related increase in variability, slower near the fovea, yielded progressively larger and more elongated clusters toward foveal and vertical-meridian SC representations. What causes this latter, unexpected, pattern remains undetermined. Nevertheless, our findings clearly suggest that the undershoot phenomenon, and related variability, originate in, or upstream of, the SC, rather than reflecting downstream, adaptive, strategies.

Introduction

Topographic maps of visual space are found in many brain areas. Some, along the geniculostriate and dorsal pathways, represent the spatial distribution of visual signals (e.g., van Essen, Newsome, & Maunsell, 1984). Others, notably in the superior colliculus (SC), as well as in the frontal eye field (FEF), carry the spatial code for orienting movements of the eye or the head (e.g., Robinson, 1972). These maps all have in common a distorted representation of visual space, owing to nonhomogeneous sampling at the level of the retina.

Citation: Vitu, F., Casteau, S., Adeli, H., Zelinsky, G. J., & Castet, E. (2017). The magnification factor accounts for the greater hypometria and imprecision of larger saccades: Evidence from a parametric human-behavioral study. *Journal of Vision*, 17(4):2, 1–38, doi:10.1167/17.4.2.

doi: 10.1167/17.4.2

Received September 17, 2016; published April 7, 2017

ISSN 1534-7362 Copyright 2017 The Authors



Because neurons in higher-level structures are relatively uniformly distributed (Polyak, 1957), the greater density of ganglion cells in the central, foveal, part of the retina results in a greater proportion of cortical and subcortical tissue being devoted to foveal compared with peripheral processing. As revealed by numerous psychophysical studies, the magnification factor (MF) strongly constrains visual perception, being responsible, among other things, for the drastic decline of acuity and contrast sensitivity with retinal eccentricity (e.g., Rovamo, Virsu, & Nasanen, 1978). Whether it also constrains oculomotor behavior has, however, remained largely unexplored (but see van Opstal & van Gisbergen, 1989b; Vitu, 1991). Using a model of the SC, in which saccades are commonly assumed to be programmed (for a review, see Girard & Berthoz, 2005), we therefore tested whether the MF accounts for the increased inaccuracy and imprecision of visually guided saccades as they become greater in size.

It has long been known that saccades made toward single peripheral targets are neither perfectly accurate nor precise but rather tend to quite systematically undershoot their target while being prone also to random errors, which make them land at variable locations across trials. Importantly, the frequency and magnitude of these systematic and random errors increase proportionally with target eccentricity (for a review, see Becker, 1989). As the target is displayed further in the visual periphery and the distance to travel becomes greater, the distribution of saccadic endpoints typically shifts toward the fovea (Lemij & Collewijn, 1989), while showing a larger spread (Frost & Pöppel, 1976), mainly along the target axis (Deubel, 1987; van Opstal & van Gisbergen, 1989b). The resulting undershoot error, of about 10% of target eccentricity on average, increases in turn the likelihood of a secondary, corrective, saccade, that most often brings the eyes on target (Becker & Fuchs, 1969). Past research led to the now widely accepted assumption that the systematic undershoot tendency reflects an adaptive visuomotor strategy. This would be aimed at reducing the risk that the eyes land past the target (Deubel, Wolf, & Hauske, 1986; Henson, 1978; see also Robinson, 1973), possibly for the sake of minimizing the overall saccade flight time and maximizing in turn the time left for clear vision, as proposed by Harris (1995). Implemented downstream of the SC, this strategy would consist in an overall adjustment of the saccadic gain (see also Becker, 1989). It would optimally avoid nontolerated target overshoot, by forcing saccades to traverse only a relatively constant percentage of the desired movement amplitudes and proportionally constraining their variability. Yet, as suggested by van Opstal and van Gisbergen (1989b) in their seminal article on saccade-endpoint scatter, an alternative and more direct explanation for the greater

spread of random errors associated with larger saccades might be in the distorted representation of visual/motor space in the SC (see also Deubel, 1987). We suspected the same might also be true for the proportional increase in the systematic undershoot bias with target eccentricity and hence that the undershoot error might form earlier than envisioned by Harris (1995).

The SC is a multilayered and integrative midbrain structure that transforms direct retinal input as well as visual and nonvisual cortical signals into a saccade program. It contains, throughout its sensory to motor layers, topographic, although distorted, maps of visual space (Ottes, van Gisbergen, & Eggermont, 1986); actually, the final topographic maps before the spatial code for a saccade, expressed in polar coordinates (amplitude and direction), are decomposed into separate horizontal and vertical motor signals/commands (Goffart, 2009). In these maps, the center of the visual field is represented in the most rostral part, whereas the periphery expands more caudally. Still, a greater surface area is devoted to the fovea, because of the MF, and also along the direction compared with the eccentricity axis, as a result of some anisotropy. Whether SC neurons discharge in response to visual stimulation, as in the superficial and intermediate layers, or prior to the execution of a saccade, as in the intermediate and deeper layers, they have large and overlapping response fields (for a review, see McIlwain, 1991). This implies that a point is not “seen” by just a single neuron but rather is coded by activity of a population of neurons with large and overlapping receptive fields (Cynader & Berman, 1972; Goldberg & Wurtz, 1972); this population forms what is traditionally called the visual point image (McIlwain, 1975). Similarly, a saccade is preceded by activity of a population of neurons coding for a large range of saccade amplitudes and directions (Sparks, Holland, & Guthrie, 1976), and that forms the motor point image. Importantly, as neurons lay more caudally, and therefore code for more peripheral locations, their response fields become increasingly larger and are also more skewed toward the periphery; this means that more caudal neurons code for an increasingly larger range of eccentricities (amplitudes) and, even more so, above than below their optimal eccentricity (amplitude). However, corresponding visual and motor point images remain unaffected because the eccentricity-related increase in response-field size and asymmetry is compensated for by the progressively smaller surface area devoted to each square-degree of visual angle: When response fields are replotted in the cells’ coordinate system, they are relatively symmetric and invariant in size (McIlwain, 1975; Ottes et al., 1986; see also Goossens & van Opstal, 2006; Munoz & Wurtz, 1995b; van Opstal, van Gisbergen, & Smith, 1990). Visual and motor point images are thus symmetrical,

and also of the same size; that is, they involve as many neurons, regardless of where a point appears in visual space and where the eyes move (see also Anderson, Keller, Gandhi, & Das, 1998; Moschovakis, Gregoriou, & Savaki, 2001).

The saccade made in response to a visual point presumably takes the eyes to the location in space that corresponds to the center of the recruited motor point image. Because the efferent mapping, in which a saccade vector is assigned to a peak of activity in the motor map, is the inverse of the afferent mapping, the saccade should thus be normometric, at least as long as visual and motor point images are in spatial register (Schiller & Stryker, 1972; Wurtz & Goldberg, 1972; but see Marino, Rodgers, Levy, & Munoz, 2008), and they are centered on the stimulus coordinates in SC space. Yet, complicating the prediction of normometric saccades is the fact that visual and motor point images are likely subject to location jitter and could possibly also show systematic location biases. Irrespective of where these random and systematic errors may originate from (i.e., from the SC or from upstream areas projecting onto the SC), they would translate, due to nonhomogeneous efferent mapping, into a greater imprecision and inaccuracy of larger saccades, respectively. Location jitter, or (random) rotation-symmetrical Gaussian variations in the location of point images, as originally assumed by van Opstal and van Gisbergen (1989b), should cause greater variations in the range of encoded saccade vectors as the stimulus is more peripheral and population activity is more caudal, yielding in turn a proportionally larger spread of landing positions, as typically observed (Frost & Pöppel, 1976). Furthermore, any systematic location bias in the population-activity profile, as we further assume, should result in a greater shift of the distribution of saccadic endpoints as the target appears at more eccentric positions; should this bias be toward the representation of the fovea, the typical linear relationship between the mean hypometria of saccades and target eccentricity would then be observed (Becker & Fuchs, 1969). Assuming this is indeed the case, the reciprocal should also be true; that is, saccadic endpoints, when projected back onto SC space, using the inverse, logarithmic afferent mapping function, should exhibit systematic and random errors that are translation invariant. This is precisely what we investigated in the present study.

Using four parametric data sets, collected while human observers made saccades toward single dot-like stimuli displayed at variable eccentricities (0.5° – 15°), and along various axes (from the horizontal to the vertical meridian) in one data set, we thus tested the following two predictions. The first, common to both the MF account and the downstream gain-adjustment hypothesis, was that saccadic endpoints,

when expressed in degrees of visual angle, would exhibit both a systematic undershoot tendency and a spread (mainly in amplitude) that would increase linearly with target eccentricity, irrespective of target direction. These relationships have already been reported in many studies but yet mainly for targets displayed in the far periphery ($\geq 5^\circ$ – 10° ; but see Abrams, Meyer, & Kornblum, 1989; de Bie, van den Brink, & van Sonderen, 1987; Evdokimidis, Tsekou, & Smyrnis, 2006; Kalesnykas & Hallett, 1994) and along the horizontal meridian (but see van Opstal & van Gisbergen, 1989b). The question thus remained whether these relationships generalize to the entire range of ordinary saccade amplitudes ($< 15^\circ$; Bahill, Adler, & Stark, 1975) and directions and to small-amplitude and vertical saccades in particular. The second prediction, made only by the MF account, was that the distributions of landing positions, when replotted in the log-scaled coordinate system of the SC, would be of the same size and shape (i.e., circular-symmetric), and also shifted by the same amount relative to the saccade target, regardless of target eccentricity and direction. Systematic and random errors should thus remain invariant across the entire representation of a visual-field quadrant. A possible exception might still be toward the vertical-meridian representation, which is shared between the two SC and typically yields half-circular population activity in both colliculi (van Opstal et al., 1990). As the geometry of the SC in humans has remained unstudied, we used Ottes et al.'s (1986) model of the SC in monkeys, to replot landing-position distributions in SC space, assuming that this might provide a reasonable first test of our hypothesis (for a similar approach, see van Opstal & van Gisbergen, 1989b).

Methods

Our study was based on a posteriori analyses of four data sets that were collected in our laboratory for other purposes (i.e., the parametric study of global and remote-distractor effects). Only the methodology and results of the control condition in which a single target stimulus was displayed at various locations in the visual field are presented here; the results of the experimental, distractor condition, in comparison with the control, have been or will be published separately (see Casteau & Vitu, 2012; see also Casteau, 2012). The consistency of the present findings across our different data sets and also in comparison with previous reports in the literature suggests that they are not specific to the experimental context in which the data were collected.

Selected data sets: Stimuli, procedure, and design

The largest, horizontal-to-vertical meridian (HM-VM) data set mapped saccade metrics over the upper right quadrant of the visual field in seven individuals. As illustrated in the left panel of Figure 1A, the single, saccade-target stimulus was displayed at variable eccentricities (2° – 11° by steps of 1°) along six different axes from the horizontal to the vertical meridian (0° , 22.5° , 45° , 67.5° , 80° , and 90°). Target eccentricity was randomly mixed within blocks of trials, but target direction was blocked. Each condition was repeated 30 times, thus yielding a total of 1,800 single-target trials (41.7% of a total of 4,320 trials) per participant.

The other three data sets, referred to as HM1, HM2, and HM3 (with HM for horizontal meridian) mapped saccade metrics along the horizontal meridian in eight individuals, respectively, but for different ranges of target eccentricities. This not only allowed us to control for possible range-related biases (e.g., Kapoula, 1985; but see Findlay, 1982; Gillen, Weiler, & Heath, 2013; Nuthmann, Vitu, Engbert, & Kliegl, 2016), but also provided a more complete description of saccadic behavior from near the center of the fovea to as far as 15° in the periphery (see Figure 1A, right panel). In HM1, the single target was presented randomly at 11 possible eccentricities (0.5° , 1° , 1.5° , 2° , 2.5° , 3° , 3.5° , 4° , 4.5° , 5° , and 6°) to the left or to the right of an initial fixation stimulus but with target direction being blocked (see Casteau & Vitu, 2012). Each condition was repeated 20 times, but because left- and right-presented targets were not analyzed separately in the present study, this resulted in 40 repetitions of each target eccentricity and a total of 440 single-target trials per participant (i.e., 39.3% of a total of 1,560 trials). In HM2 and HM3, the single target appeared always to the right of the initial fixation stimulus, at 13 (1° – 13° by steps of 1°) and 15 possible eccentricities (1° – 15° by steps of 1°), respectively. Each target eccentricity was repeated 40 times, thus resulting, respectively, in a total of 520 and 600 single-target trials per participant (31.7% and 29.4% of a total of 1,640 and 2,040 trials, respectively).

In all four experiments, the target stimulus was a small empty triangle (basis: 0.27° , height: 0.30°). In HM data sets, it was oriented either upward or downward; in HM-VM, it was always oriented upward but with or without a central lighted pixel (0.03°). On the single-target trials analyzed here, the procedure was as follows. A fixation stimulus (in the HM data sets, two vertically aligned bars of length 0.33° and width 0.03° and separated by a gap of 0.5° ; in the HM-VM data set, a cross made of two bars of length 0.33° and width 0.03°) was first presented in the central (HM1), central-left (HM2 and HM3), or lower-left part of the screen (HM-

VM). This was displayed until detection of a fixation within a vertically oriented rectangular region ($0.3^{\circ} \times 1^{\circ}$ in HM data sets and $0.3^{\circ} \times 0.4^{\circ}$ in HM-VM) around the center of the fixation stimulus. In the rare cases in which a fixation in this area was detected simultaneously with (or before) the onset of the fixation stimulus, the fixation stimulus was presented for a duration of one screen-refresh cycle. Simultaneously with the extinction of the fixation stimulus, the target was displayed (i.e., 0-ms gap [or step] paradigm). Participants were asked to move their eyes as quickly and as precisely as possible toward the target stimulus and then to press the right- or left-hand button to indicate whether the triangle was oriented upward or downward in HM data sets or whether or not it contained a central pixel in HM-VM. Button press triggered the disappearance of the target, and the simultaneous presentation in the lower (HM) or upper part of the screen (HM-VM) of two symbols (a number corresponding to the trial number, and a letter, “C” or “F,” that indicated whether the participant’s response was correct or incorrect, respectively). After a delay of 1000 ms, the symbols were removed and the next trial began.

Stimuli were displayed in white (9 cd/m^2) on a black background, using a 17-in. CRT-monitor with a 60-Hz refresh rate, positioned at a distance of 850 mm from the participant’s eyes. All data were collected using a Dual-Purkinje-Image Eye-Tracker (Ward Technical Consulting), which samples the right eye position every millisecond with an accuracy of 10 minutes of arc. The eye-movement signal was analyzed online and reanalyzed offline, using the software developed at the Catholic University of Leuven by van Rensbergen and de Troy (1993). A more detailed description of the experimental setup is presented in Casteau and Vitu (2012).

Participants were university students (13 women and six men), 18 to 23 years old, who had noncorrected, normal vision. Six participated in two of the four experiments (one in HM1 and HM2, two in HM1 and HM-VM, two in HM2 and HM3, and one in HM3 and HM-VM), and three participated in three of the four experiments (one in HM1, HM2, and HM-VM; one in HM1, HM2, and HM3; and one in HM2, HM3, and HM-VM). Experiments were approved by the committee responsible for overseeing research conducted in human subjects at Aix-Marseille University. They were performed in accordance with the ethical standards laid down in the 1964 Declaration of Helsinki, and individuals gave their informed consent prior to their participation in the experiments.

Data selection and analysis

The metrical properties of the first saccade after target onset were analyzed. Trials were considered for

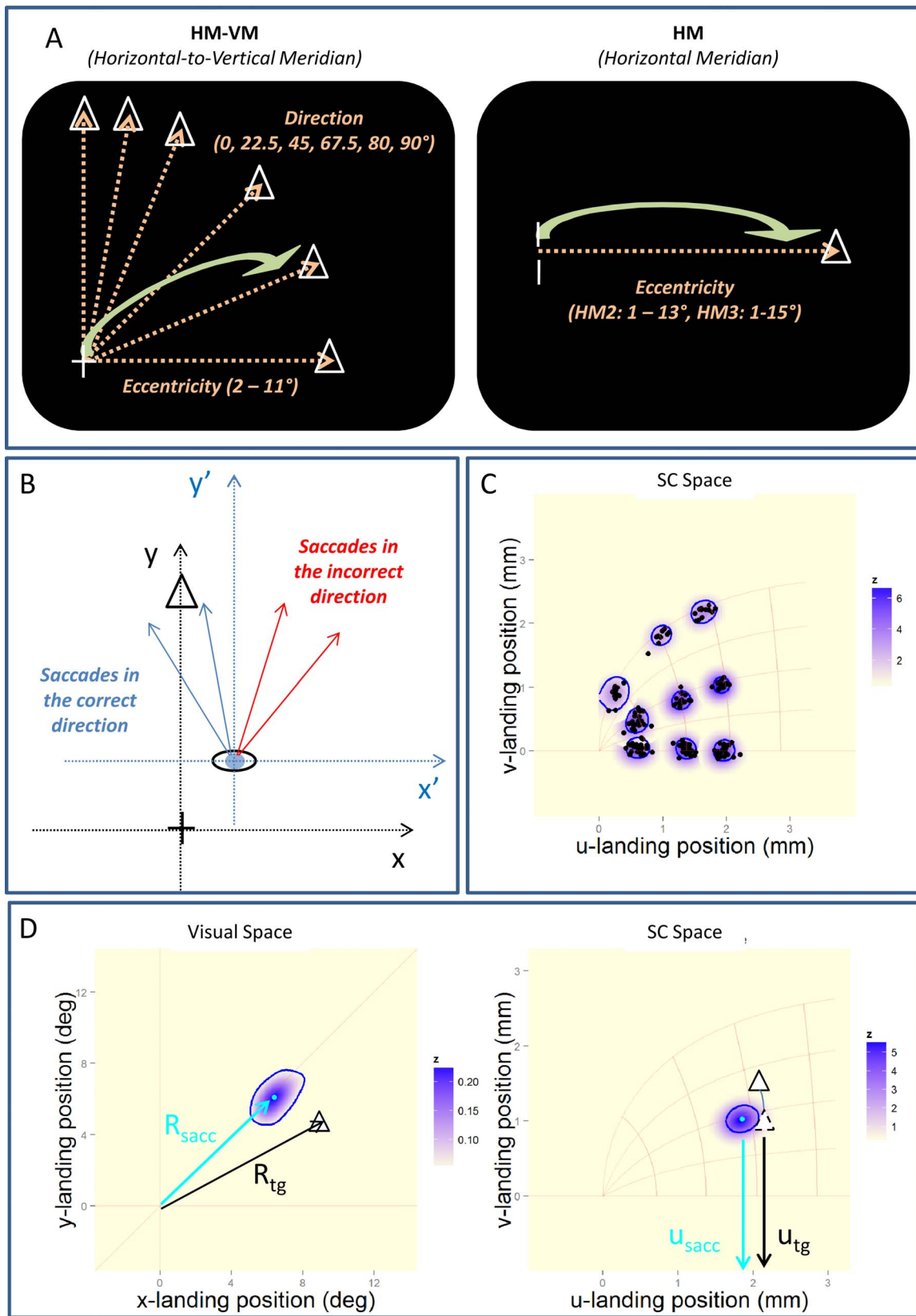


Figure 1. (A) Left panel: Illustration of the display and several of the conditions in the horizontal-to-vertical meridian data set. The initial fixation stimulus (i.e., the cross) disappeared when the target (i.e., a single triangle) appeared; this was displayed at variable eccentricities within blocks of trials (2°–11° by 1° steps) and variable directions between blocks (0°, 22.5°, 45°, 67.5°, 80°, and 90°). Right panel: Illustration of the display in HM2 and HM3 data sets. The initial fixation stimulus (i.e., two vertically aligned bars)



←

disappeared when the target (i.e., a triangle) appeared; the target, always on the horizontal meridian, was presented at variable eccentricities within blocks (1° – 13° and 1° – 15° , by 1° steps, respectively). In HM1 (not illustrated here), the display was similar except that the initial fixation stimulus was presented at the center of the screen and the target was displayed at variable eccentricities (0.5° , 1° , 1.5° , 2° , 2.5° , 3° , 3.5° , 4° , 4.5° , 5° , and 6°) to the right or to the left of fixation, depending on the block number. (B) The initial eye fixation position was almost never perfectly aligned with the fixation stimulus (cross in the example), which implied that nearly vertical saccades had a horizontal component. Both the initial saccade's landing position and the target (triangle) location were recalculated relative to the eye's effective initial fixation position (new coordinate system illustrated by dotted blue x' - and y' -axis), thus taking into account the initial eye deviation. The saccade was coded as correct if it moved the eye to the effective target side ("saccade in the correct direction"; in blue) and incorrect if it moved the eye to the opposite-target hemifield ("saccade in the incorrect direction"; in red). (C) Illustration of probability density functions and corresponding 90% isolines (in SC space in this example), with the observed data points superimposed; as shown here, both probability density function (with a fixed bandwidth) and the isolines quite accurately captured the landing-position scatter. (D) Illustration of the parameters that we used to estimate saccade accuracy. In visual space, the radius of the mode of the 90% isoline cluster (cyan dot), which corresponded to saccade amplitude (R_{sacc}), was compared with the mean eccentricity or radius (R_{tg}), across corresponding trials, of the target (black triangle). In SC space, the u -value of the mode of the 90% isoline cluster (cyan dot; u_{sacc}) was compared with the mean u -value, across corresponding trials, of the target (black triangle; u_{tg}), but after shifting the target from where it truly projected (plain triangle) onto the target's v - (direction-) axis (dashed triangle). This was done to free amplitude errors from possible direction errors.

analysis if (a) the target was displayed during a fixation and not during a saccade, (b) there was no artifact or signal irregularity in the trial, (c) there was no blink before or after the saccade, (d) a saccade was indeed launched after stimulus presentation, (e) the average eye position before saccade onset (as reestimated offline) was within less than 0.5° to the left or to the right of the center of the initial fixation stimulus and 1.33° (HM) or 1° (HM-VM) above or below the center of the fixation stimulus, (f) the saccade was not anticipatory (i.e. its latency, as measured from stimulus onset, was longer than 80 ms), and in HM-VM (g) the saccade moved the eyes within $\pm 45^{\circ}$ of the target axis; this latter criterion was relaxed in HM data sets as saccades to the opposite target hemifield could possibly occur for small target eccentricities and were worth analyzing for the current purpose. Note that performance in the perceptual task was near perfect (mean: 99.3%, 98.3%, 98.6%, and 98.4%, in HM1, HM2, HM3, and HM-VM, respectively); as errors in this task were too infrequent to affect the analyses, correct and incorrect trials were kept for analysis. After selection, a total of 2,857, 3,455, 3,936, and 8,986 cases across all participants in HM1, HM2, HM3, and HM-VM respectively, remained for analyses; this corresponded to rejection rates of 16.4%, 15.8%, 16.7%, and 26.6%, respectively. Note that similar rejection rates were previously reported for this type of paradigm and setup (e.g., Vitu, Lancelin, Jean, & Farioli, 2006).

All analyses were based on the landing position of the initial saccade, which was measured relative to the observed initial fixation position, in order to take into account the deviation of the eyes from the initial fixation stimulus before the saccade was launched (of about -0.05° , 0.09° , 0.07° , and -0.04° on average on the horizontal axis, and -0.05° , -0.41° , -0.40° , and -0.15° on the vertical axis, in HM1, HM2, HM3, and HM-

VM, respectively). The initial landing position was first expressed in degrees of visual angle and then converted into millimeters of SC space, using Ottes et al.'s (1986) logarithmic afferent-mapping function of the SC in monkeys. For a stimulus presented at an eccentricity, R , and at a meridional angle (or direction), φ , the corresponding collicular coordinates, u and v , as expressed from the rostral pole (or the representation of the fovea) along the two orthogonal axes representing, respectively, the horizontal and the deviation from the horizontal, were calculated using the following formulas:

$$u = B_u \ln \left(\sqrt{(R^2 + A^2 + 2AR \times \cos \varphi)} \right) - B_U \ln A \quad (1)$$

$$v = B_v \operatorname{atan}[(R \times \sin \varphi)/(R \times \cos \varphi + A)] \quad (2)$$

where B_u , B_v , and A were constants, set to 1.4, 1.8, and 3, respectively (i.e., the anisotropic model).

Saccades directed to a given visual hemifield (left or right) are associated with neuronal activity in the contralateral colliculus (right or left, respectively). However, for ease of representation and interpretation, and because all target stimuli were not presented within the right visual hemifield (as in HM1), the landing positions of the saccades that moved the eye in the correct direction were all represented in (the upper part of) the right colliculus, whether these were rightward or leftward saccades; as shown in separate analyses, target direction indeed had no significant effect (see Casteau & Vitu, 2012). In the particular case in which a stimulus was displayed on the upper vertical meridian, saccades were considered as being in the correct direction when they moved the eye to the upper part of the screen and also to the side where the target appeared relative to the

initial eye-fixation location, which was almost never perfectly aligned with the vertical meridian (see Figure 1B). Thus, when the vertical target ended up being in the right (or left) hemifield and the eye moved to the upper right (left) part of the screen, the saccade was considered as being in the correct direction, and its landing position was represented in the upper part of the right SC, whereas it was incorrect and represented in the upper left SC when directed to the left (right) side. Similarly, horizontal saccades in the correct direction not only moved the eyes to the side where the target was presented but also to the upper/lower visual hemifield where it appeared, again relative to the initial fixation location; these were represented in the upper part of the right SC. This remapping procedure allowed us to minimize potential biases toward one particular part/side of the screen, which may in fact result from systematic fixation biases relative to the initial fixation stimulus. Note, however, that a pattern of data very similar to that reported below was obtained without remapping.

To characterize for each individual in each condition, the bivariate distributions of initial landing positions in both visual (x,y) and collicular (u,v) space, but without making any assumption of their shape (e.g., whether or not they were normally distributed and unimodal), the procedure advocated by Castet and Crossland (2012) for estimating fixation stability was applied. First, the probability density function of landing positions was estimated, using the kernel density estimation (ks package in the R software; R Core Team, 2012), with a fixed kernel bandwidth (0.3° and 0.02 mm in visual and SC space, respectively); note that similar findings were obtained when the optimal bandwidth was determined using adaptive procedures, and also, as illustrated in Figure 1C, that the shape of the probability density functions matched the scatter of the observed landing positions. Then, isolines (or contour lines) were computed and were set to delineate the region(s) in space that contained 90% of the data points with the highest density estimate (see Figure 1C). This allowed us, at the same time, to filter out the small, isolated clusters, which were mostly located near the initial fixation stimulus and corresponded to initial saccades of small amplitude ($\leq 2^\circ$; about 1.09%, 0.83%, 0.45%, and 1.16% of all initial saccades in conditions where the target appeared at an eccentricity greater than 3° in HM1, HM2, HM3, and HM-VM). When two (or more) separate clusters remained, the largest (which corresponded to the cluster with the highest density estimate at its mode) was kept for further analysis, thus providing the most representative region in space where the eyes initially landed. However, in the particular case where two clusters were detected in two opposite colliculi, as was the case when the target was displayed along the vertical meridian (see the Results

section), the area considered for further analysis was the area corresponding to saccades in the correct horizontal direction (i.e., the saccades directed to the target side given the initial eye deviation from the fixation stimulus; see above); this actually corresponded to the largest area in most individuals (see Results). Note that this also allowed a more direct comparison with the landing-position distributions associated with targets displayed on other axes, which corresponded almost exclusively to saccades in the correct direction. Yet, as verified in complementary analyses, this procedure was not responsible for the specific data pattern observed with targets displayed on and near the vertical meridian (see Results).

The mode of the selected isoline cluster, which indicated where the eye most frequently landed relative to the initial fixation position, was used to estimate the accuracy of saccades. Because saccade metrics are best described in a polar coordinate system (Deubel, 1987; van Opstal & van Gisbergen, 1989b), both the radial amplitude of the initial saccade (R_{sacc}) and its direction (φ_{sacc}) were computed based on the (x,y) coordinates of the mode in visual space, with R_{sacc} corresponding to the square root of the sum of squares of x and y and φ_{sacc} corresponding to the angle formed by R_{sacc} (see Figure 1D, left panel). To estimate saccade accuracy as a function of the effective eccentricity (R_{tg}) and direction (φ_{tg}) of the target, both R_{tg} and φ_{tg} were recalculated on each trial, taking into account the initial eye deviation relative to the fixation stimulus (exactly as was done for initial landing positions); these were then averaged over all trials in a given condition for comparison with the corresponding saccade parameters. Two estimates of saccade accuracy in visual space were derived: (a) the *amplitude error* (or difference in degrees of visual angle between the radius of the mode and mean target eccentricity) and (b) the *gain* (or ratio of radius of the mode and mean target eccentricity). Because Ottes et al.'s (1986) afferent-mapping function projects R - and φ -retinal coordinates onto corresponding u - and v -collicular coordinates, the u -coordinate of the estimated mode was used to approximate saccade amplitude in SC space. To compute the corresponding amplitude error, the u -coordinate of the mode was subtracted from the mean across trials of the u -coordinate of the effective target eccentricity (relative to the initial fixation position) but after shifting the target on the collicular saccade axis (see Figure 1D, right panel). The latter correction was done to free amplitude-error estimates from possible direction errors; indeed, the u -value that corresponds to a given target eccentricity (or saccade amplitude) varies depending on target (saccade) direction.

The *area* subtended by the selected isoline cluster was also computed in both visual and SC space. This was used as a first index of the spread of initial landing

position distributions. To further characterize visual and collicular landing position distributions, an ellipse was fitted to the selected isoline area. The estimated *length of major and minor axes of the ellipse* provided additional estimates of the spread of the distribution, along and perpendicular to the target axis, as we will see; following van Opstal and van Gisbergen (1989b), we will refer to these as *eccentricity* and *direction axes*. Estimating major- and minor-axis lengths also allowed us to compute the area subtended by the ellipse and to estimate in turn the quality of the fit, by comparison with the estimated area of the isoline cluster before the ellipse was fit. This was relatively good and comparable across individuals and data sets, as well as between visual and SC spaces (mean residuals: 0.00242 deg² and 0.00012 mm², 0.00884 deg² and 0.00013 mm², 0.00442 deg² and 0.00010 mm², 0.01589 deg² and 0.00045 mm², respectively in HM1, HM2, HM3, and HM-VM data sets). The slope of the relationship between the area subtended by the fitted ellipse and the 90% isoline area was close to 1 (visual space: 0.995, 0.985, 0.996, and 0.987; SC space: 1, 0.999, 1 and 0.987; for HM1, HM2, HM3, and HM-VM, respectively), and the proportion of variance explained (R^2) was greater than or equal to 0.9995 in both visual and SC space.

The *ratio of the ellipse's major and minor axes* was then computed to estimate the elliptic versus round shape of visual and collicular distributions. Finally, the level of asymmetry of visual and collicular distributions and their skewness (or signed asymmetry) along eccentricity and direction axes, and hence in terms of saccade amplitude and direction, were estimated. The absolute *asymmetry* corresponded to the Euclidian distance between the estimated center of the selected isoline cluster (see below) and its mode. The *amplitude skewness* in visual space corresponded to the difference between the eccentricity of the center and the eccentricity of the mode of the selected isoline cluster; in SC space, it corresponded to the difference between corresponding u-coordinates. It was negative when the distribution was skewed toward the (representation of the) fovea and positive when skewed in a direction away from the (representation of the) fovea. *Direction skewness* in visual space corresponded to the distance, in degrees of visual angle, between the axis of the center and the axis of the mode of the selected isoline cluster; in SC space, it corresponded to the difference between corresponding v-coordinates. It was negative when the distribution was skewed toward the (representation of the) horizontal meridian or a position below it. Three different estimates of the center of the selected isoline cluster were used: (a) the estimated center of the fitted ellipse, (b) the mean of the sampling points that were used for computation of the isoline area, and (c) the raw mean of all initial landing positions, but after exclusion of the population of small-amplitude sac-

ades that kept the eye in the region of the initial fixation stimulus. All three center estimates yielded similar asymmetry/skewness patterns as a function of the tested variables, but the first two were a bit less sensitive, leading to slightly smaller estimates of asymmetry and skewness compared with the third, raw mean-based estimate of the distribution's center. Only the results for the latter are presented below.

For each data set and each of the above-defined dependent variables in visual and SC spaces (amplitude error, gain, area, length of major and minor axes of the fitted ellipse, ellipse-axis ratio, asymmetry, and amplitude/direction skewness), as well as saccade latency, linear mixed-effect (LME) modeling was conducted using the “lme” function of the nlme package in R (Pinheiro & Bates, 1996); because of their random structure, LME models present the advantage of taking into account intersubject variability in the size and direction of the effects. For both visual and collicular analyses, the top-down approach recommended by Zuur, Ieno, Walker, Saveliev, and Smith (2009) was adopted to find the model that best accounted for the data. The first step consisted of finding the optimal random structure, using the most complex fixed component (with all explanatory variables and as many interactions as possible), and comparing the fit (using Akaike's Information Criterion [AIC]) of all possible random structures (i.e., none, random intercept by participants, random effect of each [and each combination of] explanatory variable[s] by participants). The second step consisted of finding the optimal fixed structure, using the previously selected optimal random structure (i.e., that with the smallest AIC value). For the HM-VM data set, the starting fixed structure comprised both the linear and the quadratic components of the effect of target eccentricity, the (linear) effect of target direction, and the corresponding interactions (Eccentricity \times Direction and Eccentricity² \times Direction). For HM data sets, the starting fixed structure comprised both the linear and the quadratic components of the effect of target eccentricity. In all analyses, the predictor(s), that is, eccentricity in HM data sets and eccentricity and direction in the HM-VM data set, were entered as continuous variables. Because the smallest eccentricity in the range of tested eccentricities was different from zero and differed between data sets, this variable was centered on its mean. The fixed effects of optimal LME models are fully reported in Tables A1–A10 of Appendix 1. Only significant ($p \leq 0.05$) intercept and slope estimates are reported in the Results section; for each model, the optimal random structure is presented in the corresponding table's legend. Note that nonsignificant effects and interactions are often dropped when gradually converging toward an optimal fixed structure; they were thus not systematically reported in the

tables, all depending on the outcome of the optimal fixed-structure procedure.

Results

Overall description of probability density functions in visual and SC spaces

In Figures 2A–C and 3A–C, individual probability density functions and corresponding 90% isolines are shown for a subset of target eccentricities and directions in the HM-VM, HM1, and HM3 data sets. These first reveal that initial landing positions, when expressed in degrees of visual angle, formed single clusters, centered on the eccentricity axis (Figures 2A and 3A). In the rare cases two clusters formed, the additional cluster was much smaller and negligible (e.g., Figures 2A, Participants 2 and 6). In SC space, thus when initial landing positions were log transformed and converted into millimeters of collicular surface, the distributions were also unimodal (Figures 2B–C and 3B–C), except in the vertical condition, where they tended to have two separate, bilateral, modes (Figures 2B–C).

This is further illustrated in Figure 4A–B, which shows that for most individuals and eccentricities in the vertical condition, except in a few cases in which the target appeared near the fovea (2° – 3°), the systematically unimodal and vertically aligned distributions in visual space split into two bilateral distributions in SC space. The two clusters of a pair were of about the same size in Participants 1 and 4. However, for all other five participants, they were of unequal sizes, with the largest area corresponding to saccades either in the correct direction (i.e., to the side where the target was truly located, given the initial eye deviation from the fixation stimulus), as for Participants 2–3 and 5–6, or in the incorrect direction, as for Participant 7. These findings are consistent with Robinson's (1972) original proposal that purely vertical saccades result from balanced activity in the two colliculi, as well as previous electrophysiological data showing that neurons near the representation of the vertical meridian code for both ipsilateral and contralateral saccades (e.g., van Opstal et al., 1990). Yet the response fields of SC neurons cross the vertical meridian only slightly (Goldberg & Wurtz, 1972; see also van Opstal et al., 1990). Accordingly, the visual and collicular landing position distributions for targets displayed on the 80° axis (not shown here), thus only 10° away from the vertical meridian, were all unimodal, and all collicular distributions but one near the representation of the fovea (i.e., 2° eccentricity in Participant 7) were unilateral. Moreover, the distributions associated with

2° targets on other axes ($\leq 67.5^{\circ}$) were all unilaterally distributed (see Figure 2B–C). Only for horizontal targets displayed within less than 1° from the center of the fovea, as in HM1, did the probability density functions slightly expand to the nontarget hemifield, and still only one of the corresponding 90% isolines crossed the vertical-meridian representation (see Figure 3C). It thus seems that bilateral collicular representations are almost exclusively specific to stimuli displayed on (and very near to) the vertical meridian and hence to the programming of (nearly) vertical saccades.

The comparison between the probability density functions in visual and SC spaces reveals other important differences, notably in the shape and size of the distributions as well as in the (mis)alignment of their mode with the visual target; these differences are actually critical to distinguish between MF and downstream, gain-adjustment, hypotheses. First, as shown in Figures 2A and 3A, initial landing positions expressed in degrees of visual angle mainly spread along the eccentricity axis but showed little variability perpendicular to that axis, thus meaning that saccade amplitude was more variable than saccade direction (Deubel, 1987; see also van Opstal et al., 1990; van Opstal & van Gisbergen, 1989b). The phenomenon, also assessed by the elliptical shape of the corresponding contour lines, was further accentuated at greater eccentricities. This indicates that larger saccades were associated with greater variability but mainly in amplitude. In contrast, as shown in Figures 2B–C and 3B, corresponding bivariate distributions in SC space tended to be circular in shape, which was to be expected given the anisotropic representation of visual space in the SC (see Ottes et al., 1986). Furthermore, as predicted by nonhomogeneous afferent/efferent mapping, and hence the MF hypothesis, both the probability density functions and the 90% isolines showed no systematic variation in size for a large range of target eccentricities and directions. Still, distributions closer to the representation of the vertical meridian, as well as the fovea, tended to be more widely spread, particularly along the eccentricity-axis representation; these were in turn more elliptic than circular in shape, as further illustrated in Figure 3C for HM1 (for a similar report, see van Opstal & van Gisbergen, 1989b). This was predicted neither by the MF nor the downstream, gain-adjustment, hypothesis.

Finally, Figures 2A and 3A show that in most individuals, and irrespective of target direction, the distributions of landing positions in visual space that were associated with the most peripheral targets (i.e., 6° and 11° targets in HM-VM and 8° and 15° targets in HM3) did not peak at the location of the target, but they peaked in front of it; the undershoot error was greater for larger eccentricities, exactly as in previous studies (e.g., Becker & Fuchs, 1969; Frost & Pöppel,

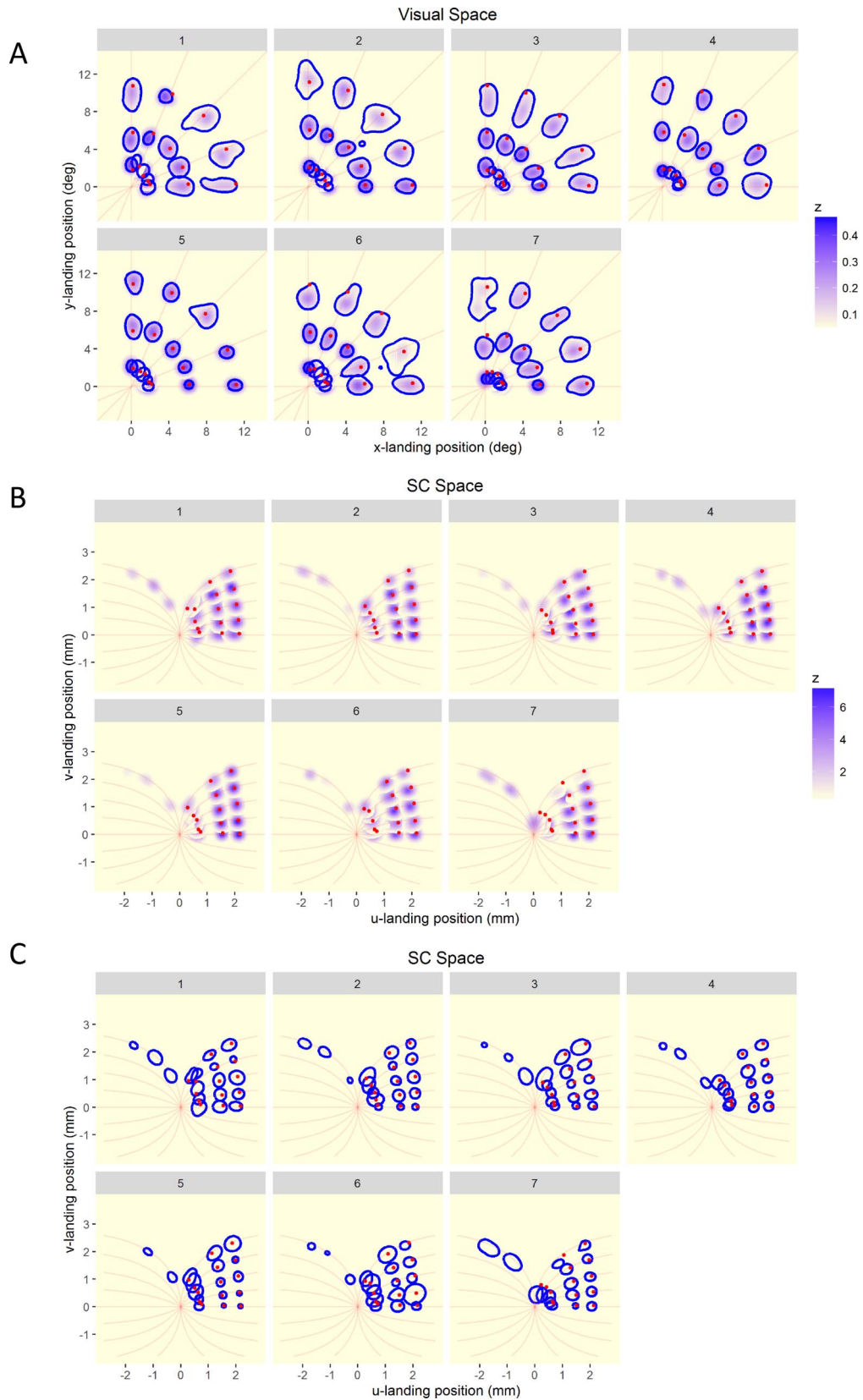


Figure 2. Two-dimensional probability density functions of the landing positions of initial saccades in degrees of visual angle (A) and millimeters of SC space (B) and corresponding 90% isolines (A and C, respectively), for each participant, but a subset of conditions in HM-VM data set. In these conditions, the visual target (red dot) was displayed at 2°, 6°, and 11° eccentricities on 0°, 22.5°, 45°, 67.5°, and 90° axes.

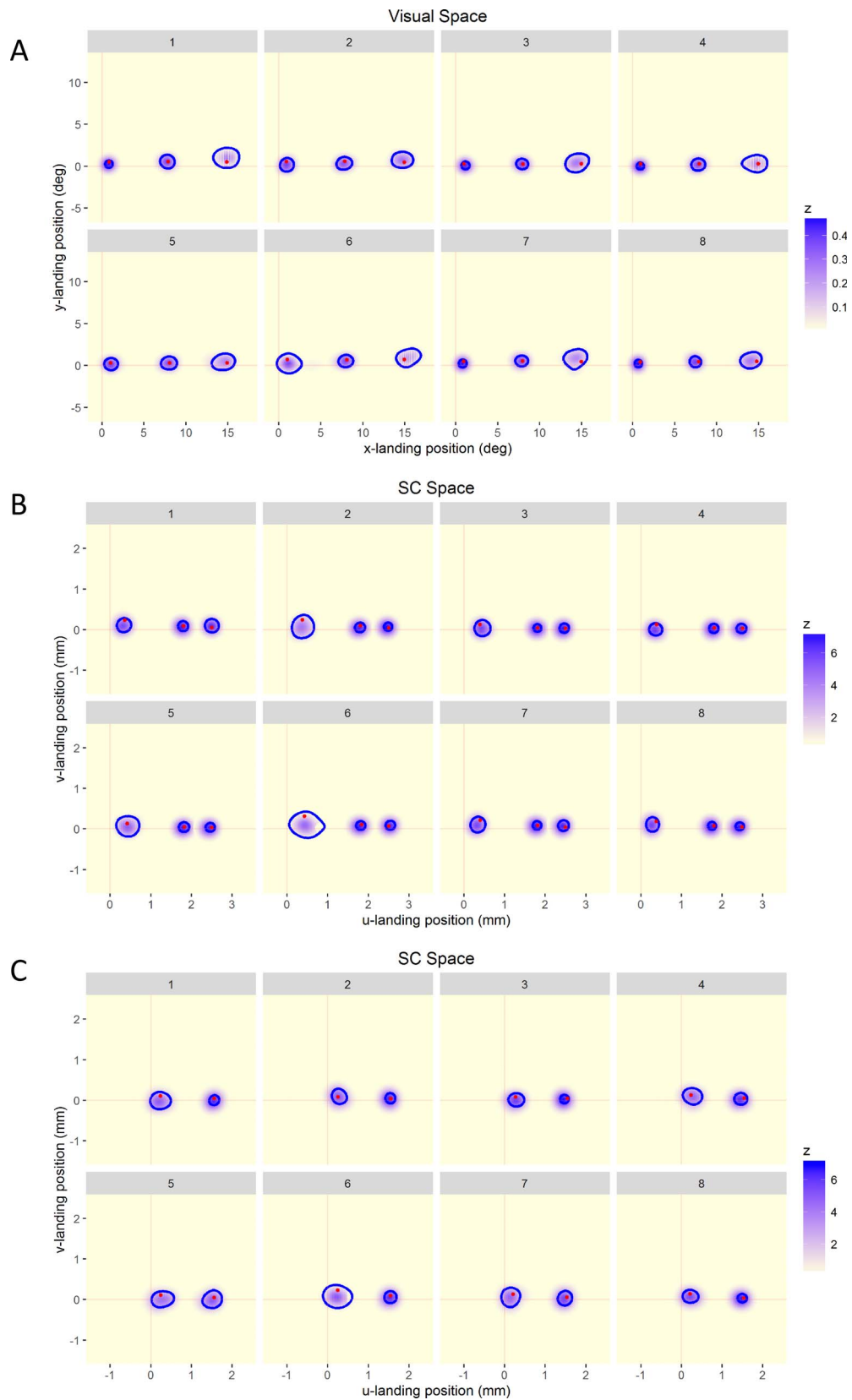


Figure 3. Two-dimensional probability density functions of the landing positions of initial saccades in degrees of visual angle (A) and millimeters of SC space (B, C) and corresponding 90% isolines for each participant, but a subset of conditions in HM3 (A, B) and HM1 (C) data sets. In these conditions, the visual target (red dot) was displayed at 1°, 8°, and 15° eccentricities on the horizontal meridian in HM3 (A, B) and 0.5° and 6° eccentricities on the horizontal meridian in HM1 (C).

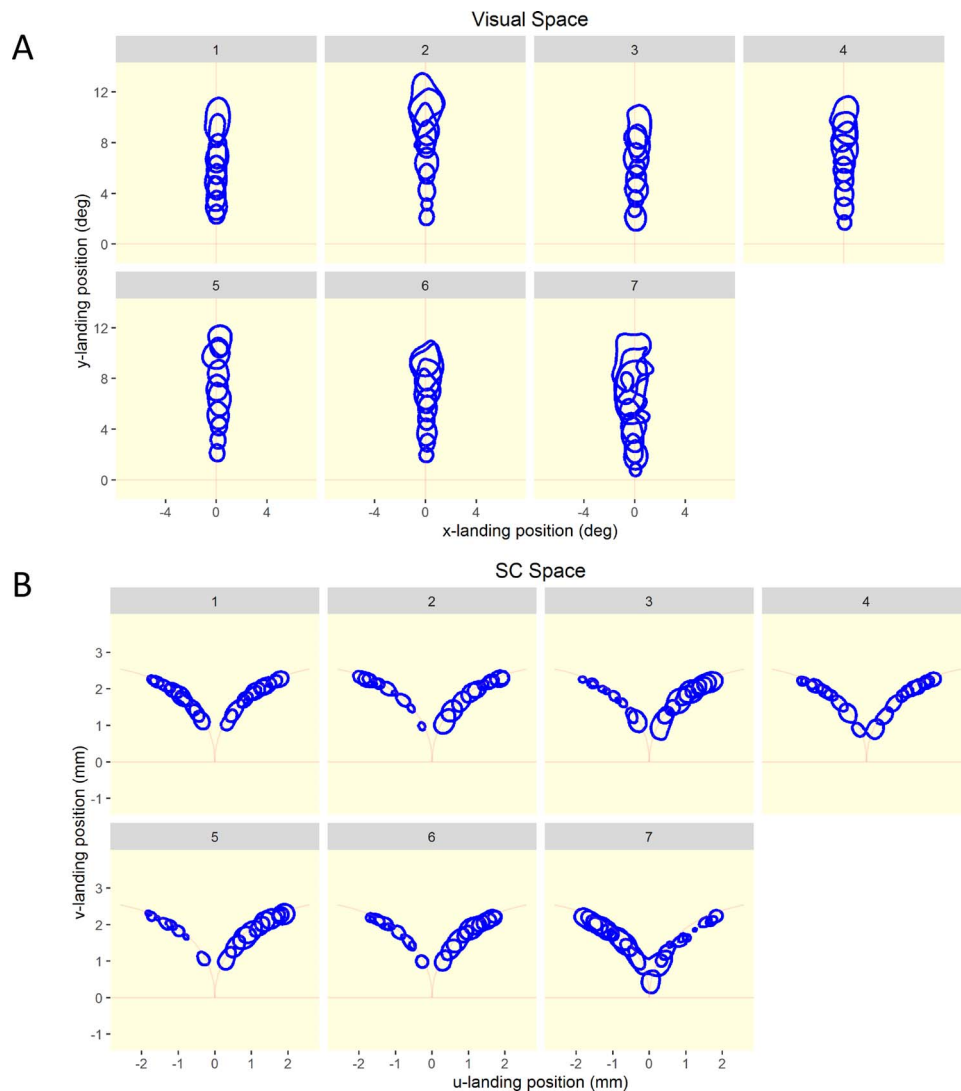


Figure 4. Ninety percent isolines of the landing positions of initial saccades in degrees of visual angle (A) and millimeters of SC space (B) for each participant, in the vertical condition of the HM-VM data set. The visual target was displayed at 2° – 11° eccentricities.

1976). The novel finding, as shown in Figures 2B–C and 3B–C, is that this pattern did not fully replicate in SC space. Although an undershoot error was maintained, as suggested by the systematic shift of the densest part of the distributions relative to target location, the error appeared to be relatively invariant across the different target eccentricities and directions, as would be expected under an MF account.

To put MF and downstream, gain-adjustment, hypotheses to a stronger test, further analyses were conducted to estimate the spread, the shape, the (as)symmetry, and the undershoot error of saccade-endpoint scatter as a function of target eccentricity and direction, in both visual and SC spaces. The results of these analyses are reported in the next four sections. In an additional section, control analyses are reported; these were aimed at determining whether the observed

properties of landing-position distributions held when saccade latency was taken into account.

The spread of landing-position distributions

The spread of landing positions was estimated in each individual and condition, using three indexes, the area subtended by 90% isolines, and the lengths of both the major and the minor axes of the corresponding fitted ellipses. In Figures 5 and 6, the means across individuals for all three indexes in visual and SC spaces were plotted as a function of target eccentricity and direction in HM-VM and target eccentricity in HM data sets, respectively. Results of the corresponding LME analyses are summarized in Tables A1–A3 of Appendix 1, with the optimal random structure being detailed in the table legends. In all data sets, the

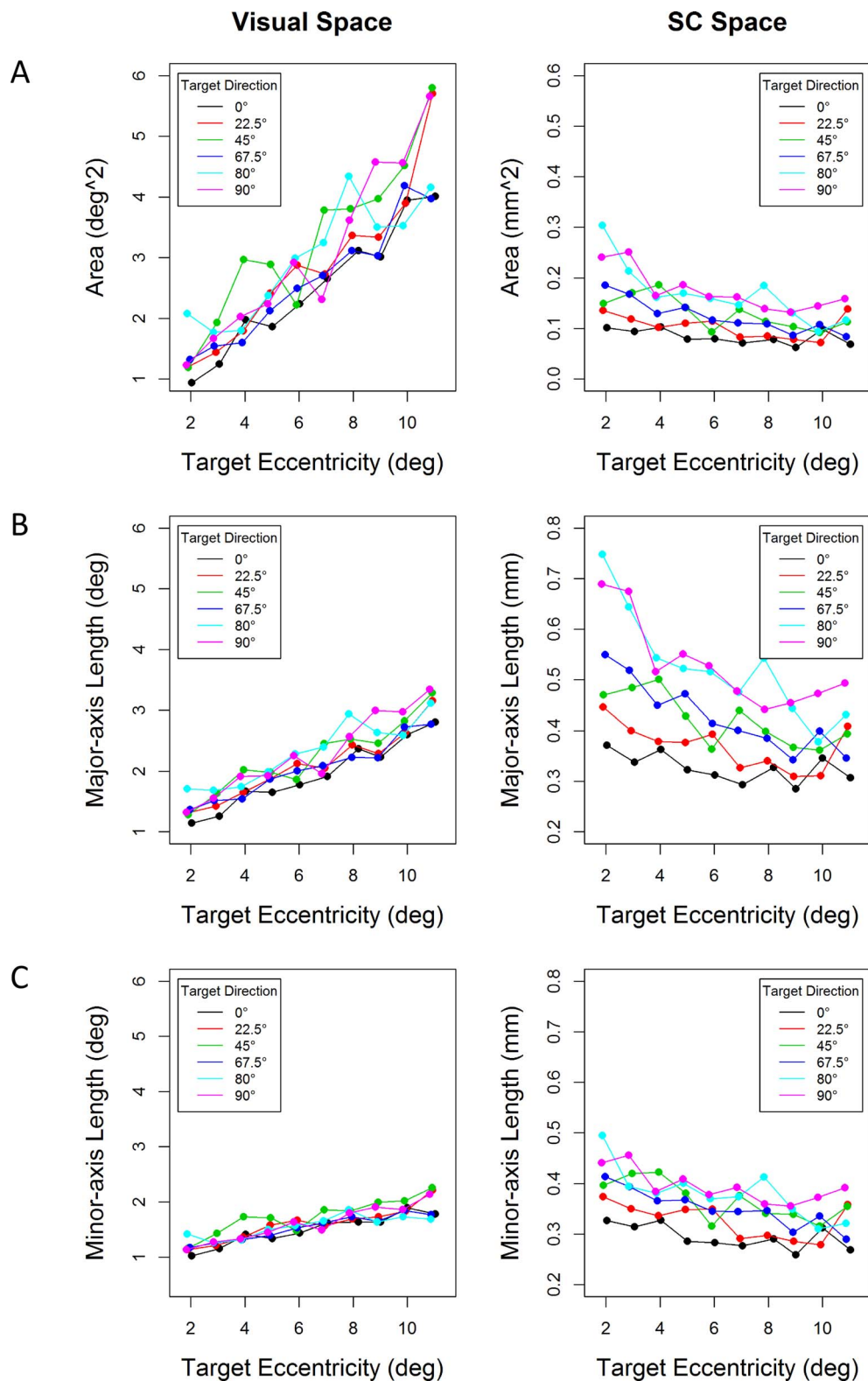


Figure 5. Mean area subtended by 90%-isoline clusters of landing positions (A), and mean length of major (B) and minor (C) axes of the corresponding fitted ellipses in (squared) degrees of visual angle (left panels) and (squared) millimeters of SC space (right panels) as a function of target eccentricity (in degrees) and target direction (in degrees; different colors) in the HM-VM data set.

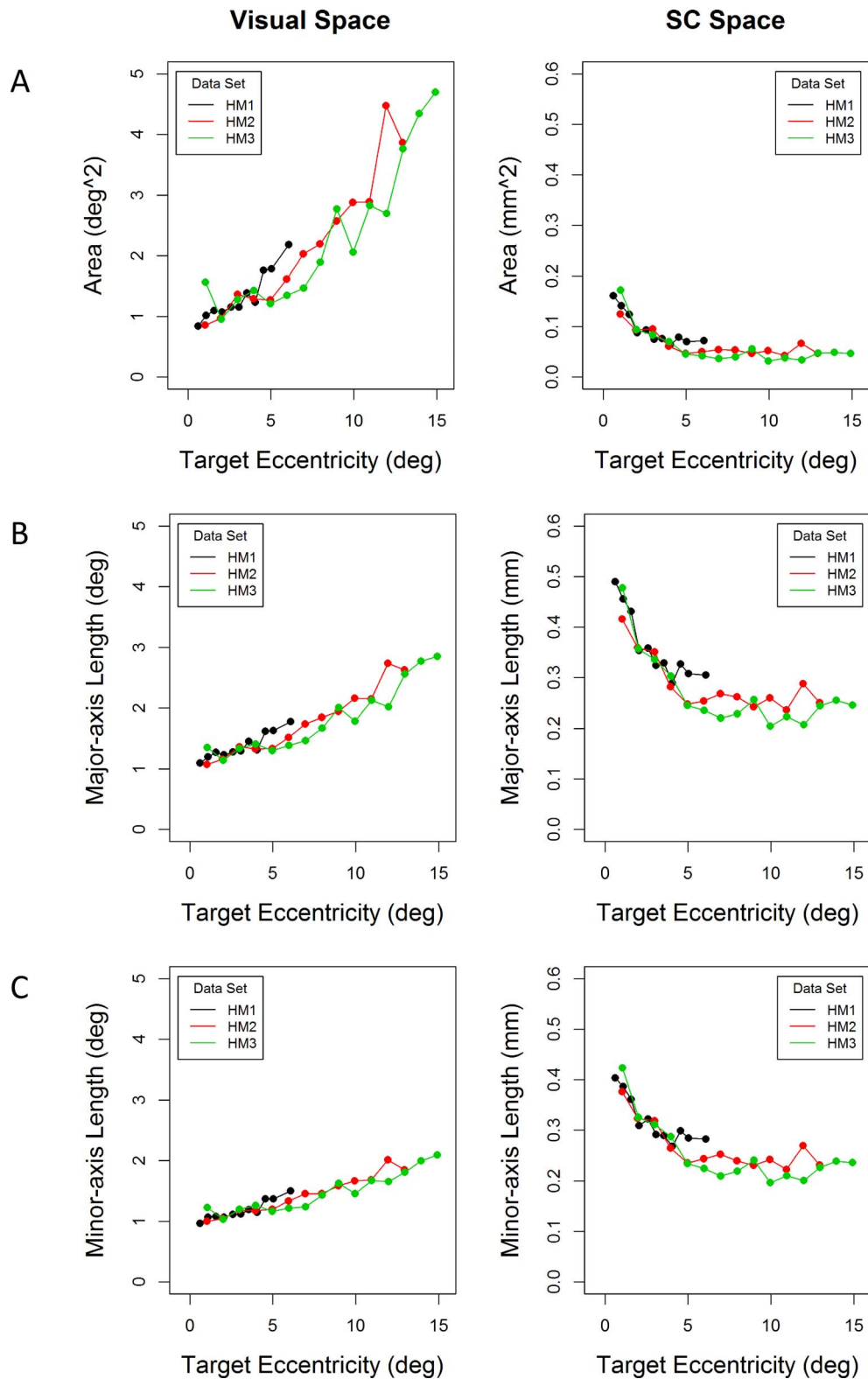


Figure 6. Mean area subtended by 90%-isoline clusters of landing positions (A), and mean length of major (B) and minor (C) axes of the corresponding fitted ellipses in (squared) degrees of visual angle (left panels) and (squared) millimeters of SC space (right panels) as a function of target eccentricity (in degrees) in HM1 (black), HM2 (red), and HM3 (green) data sets; the target always appeared on the horizontal meridian.

variability of landing positions in visual space, as measured by the estimated area encompassed by 90% isolines, increased gradually with target eccentricity (see Figures 5A and 6A, left panels). In the HM-VM data set, this relationship was linear, as confirmed by the significant linear component of the effect of eccentricity, and this held true irrespective of target direction, as assessed by the nonsignificant interaction between eccentricity and direction and the lack of an effect of direction (see Appendix 1, Table A1A). The positive 0.36 slope indicated that the landing-position cluster more than doubled its size with every 2° increment of target eccentricity. In HM1, HM2, and HM3 data sets, the slope was slightly less (estimates: 0.211, 0.274, and 0.241, respectively), and the quadratic component was also significant (estimates: 0.036, 0.017, and 0.025, respectively). This latter trend suggested a smaller increase of area size per degree eccentricity within an extended foveal region (0°–5°) that was probably best captured in HM data sets because eccentricities smaller than 2° (the minimal eccentricity in the HM-VM data set) were also tested.

The mean length of major and minor axes of the fitted ellipses showed about the same pattern (see Figures 5B–C and 6B–C, left panels), which is a linear increase with target eccentricity that was invariant across target directions in the HM-VM data set and a linear and in some instances quadratic increase in HM data sets (see Appendix 1, Tables A2A–A3A). Interestingly, the major-axis length increased faster with target eccentricity, about twice as fast, compared with the minor-axis length (linear slope estimates: 0.116 vs. 0.085, 0.135 vs. 0.079, 0.117 vs. 0.068, and 0.172 vs. 0.082 in HM1, HM2, HM3, and HM-VM data sets, respectively; quadratic slope estimates: none vs. 0.011, 0.006 vs. none, and 0.009 vs. 0.005, for HM1, HM2, and HM3, respectively). This suggested, in accordance with van Opstal and van Gisbergen's (1989b) previous findings, that the variability in saccade amplitude (as measured by the length of the ellipse's major axis) increased more with target eccentricity compared with the variability in saccade direction (i.e., the minor-axis length).

According to the MF hypothesis, which assumes that nonhomogeneous afferent/efferent mapping is responsible for the linear increase in the imprecision of saccades with target eccentricity, the spread of landing positions replotted in SC space should remain unaffected by eccentricity. Accordingly, as shown in the right panels of Figure 6A–C for HM data sets, the estimated 90%-isoline area and the length of both the major and the minor ellipse axes remained constant into the periphery. Yet all three measures increased as the target moved from an eccentricity of about 5° toward the center of the fovea (0.5° and 1° in HM1 and HM2/3, respectively), thus still showing a trend

opposite to that in visual space. This was further assessed by the negative-slope estimates for the linear effect of eccentricity in all three dependent variables and data sets (HM1: –0.017, –0.037, and –0.024; HM2: –0.005, –0.010, and –0.009; HM3: –0.005, –0.011, and –0.010 for area, major-axis length, and minor-axis length, respectively; see Appendix 1, Tables A1B–A3B), as well as the significant quadratic trend (HM1: 0.006, 0.010, and 0.007; HM2: 0.001, 0.002, and 0.002; HM3: 0.001, 0.003, and 0.002 for area, major-axis length, and minor-axis length, respectively); note that the slopes were only slightly larger for the major- compared with the minor-axis length. In the HM-VM data set, the three estimates of the spread also showed little variation with target eccentricity, apart from a gradual increase from eccentricities of about 4°–5° to the smallest, 2° eccentricity, and even more so as the target moved from the horizontal to the vertical meridian (see Figure 5A–C, right panels). In all three dependent variables, the quadratic component of the effect of eccentricity was significant (0.001, 0.003, and 0.001 for area, major-axis length, and minor-axis length, respectively), as well as the effect of direction (0.001, 0.002, and 0.001 for area, major-axis length, and minor-axis length, respectively). The anisotropy of the spread increase within the extended foveal region was still greater along the eccentricity axis, as further assessed by the significant interaction between eccentricity and direction only for the area and the major-axis length (–0.0001 and 0.0002, respectively) but not for the minor-axis length.

It is unlikely that the lack of spread invariance across the entire range of target eccentricities in SC space was an artifact of Ottes et al.'s (1986) logarithmic transformation. Indeed, as we have seen, the variability of landing positions in visual space, that is, before data were log transformed, showed a mirror-image quadratic trend, with a slower increase within about 5° from the center of the fovea. This is further illustrated in the left panel of Figure 7A, where the observed relationship between eccentricity and major-axis length in visual space, for the two most representative HM (2–3) data sets, was compared with that predicted by a constant jitter along the representation of the eccentricity axis in SC space. When using, as an approximation for the amount of jitter, the mean across the two data sets of LME intercept estimates of major-axis lengths in SC space (when all variables were at their reference, mean, value; 6.96° and 7.97°), the predicted slope (gray line) was similar to that observed above, but not below, an eccentricity of about 5° (red and green lines); this was about the eccentricity at which spread invariance broke down in SC space (see right panel). The same was true for the eccentricity-related increase in minor-axis length (Figure 7B).

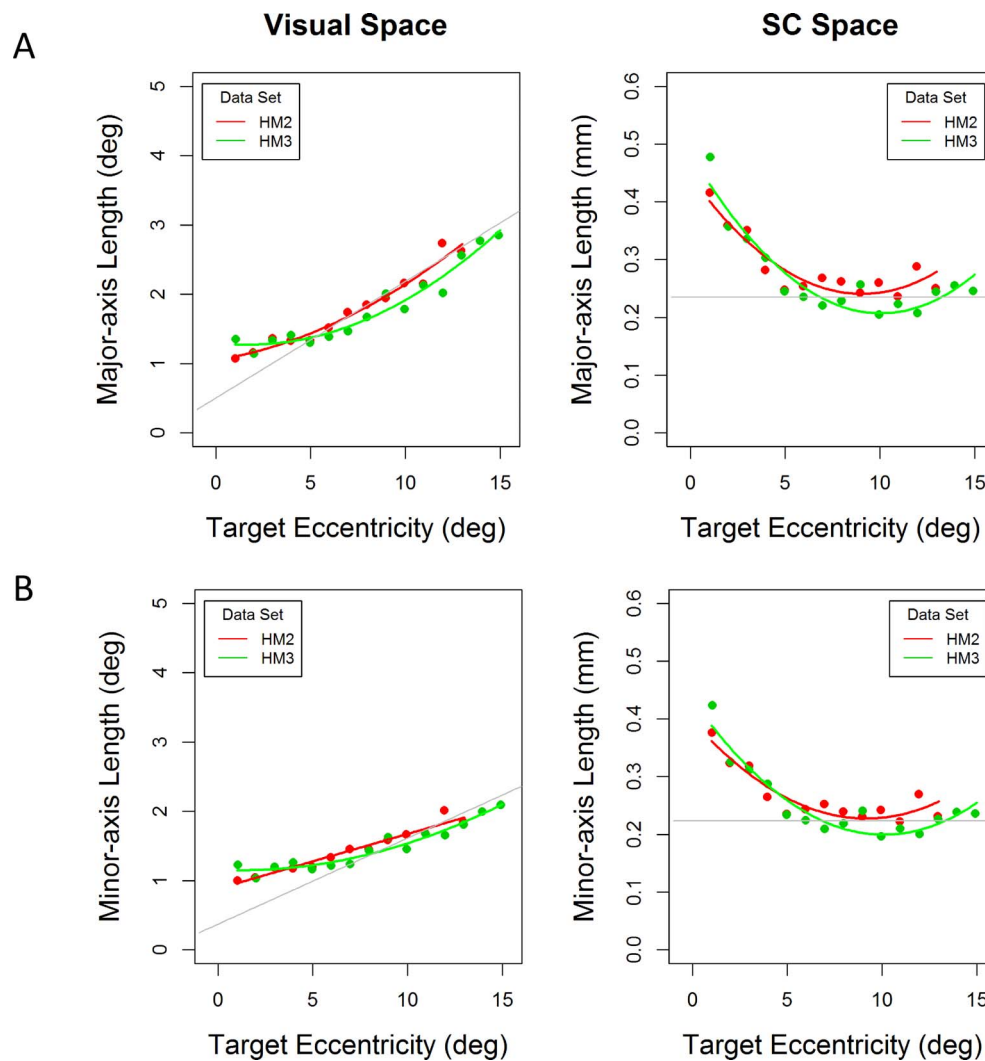


Figure 7. Mean length of major (A) and minor (B) axes of the ellipses fitted to 90%-isoline clusters of landing positions, expressed in degrees of visual angle (left panels) and millimeters of SC space (right panels), as a function of target eccentricity (in degrees) in HM2 (red) and HM3 (green) data sets. In left panels, the slope of the relationships predicted by a constant jitter in SC space (see horizontal gray line in right panels) is represented in gray.

Importantly, as revealed by comparison of Figures 5 and 6, the collicular spread increase at smaller eccentricities in HM data sets was larger than that observed along the horizontal meridian in HM-VM, while being of about the same magnitude as in the HM-VM vertical condition. This could result from the smallest eccentricity in HM data sets (0.5° – 1°) being smaller than in HM-VM (2°), combined with the fact that a given target is represented further away along the rostrocaudal axis as it moves from the vertical to the horizontal meridian (see Figure 1D). In line with this suggestion, Figure 8A shows that when the mean lengths of major and minor ellipse axes (in millimeters of SC space) in HM-VM were replotted as a function of the target's u -collicular coordinate, the data points corresponding to different target directions overlapped more (for comparison, see Figure 5B–C) and showed

an overall increase as u -values went from about 1 mm to near 0 mm. In addition, as shown in Figure 8B, the relationship for targets on the horizontal meridian in HM-VM was quite similar to that obtained in the other HM data sets; all nicely overlapping curves showed a gradually increasing spread of landing positions as u -values decreased, starting again from about 1 mm. This suggests that how far, from the rostral pole, the target projects may be a critical variable in determining the variability of saccadic endpoints. Yet this clearly cannot be the only explanatory variable for the gradual increase of the spread of landing positions from the 0° to the 90° axis, because this was still visible even after controlling for the target's u -coordinate (see Figure 8A). The fact that small-eccentricity targets are more likely to yield bilateral population activity in SC space near the vertical meridian (see Figures 2B–C and 4B)

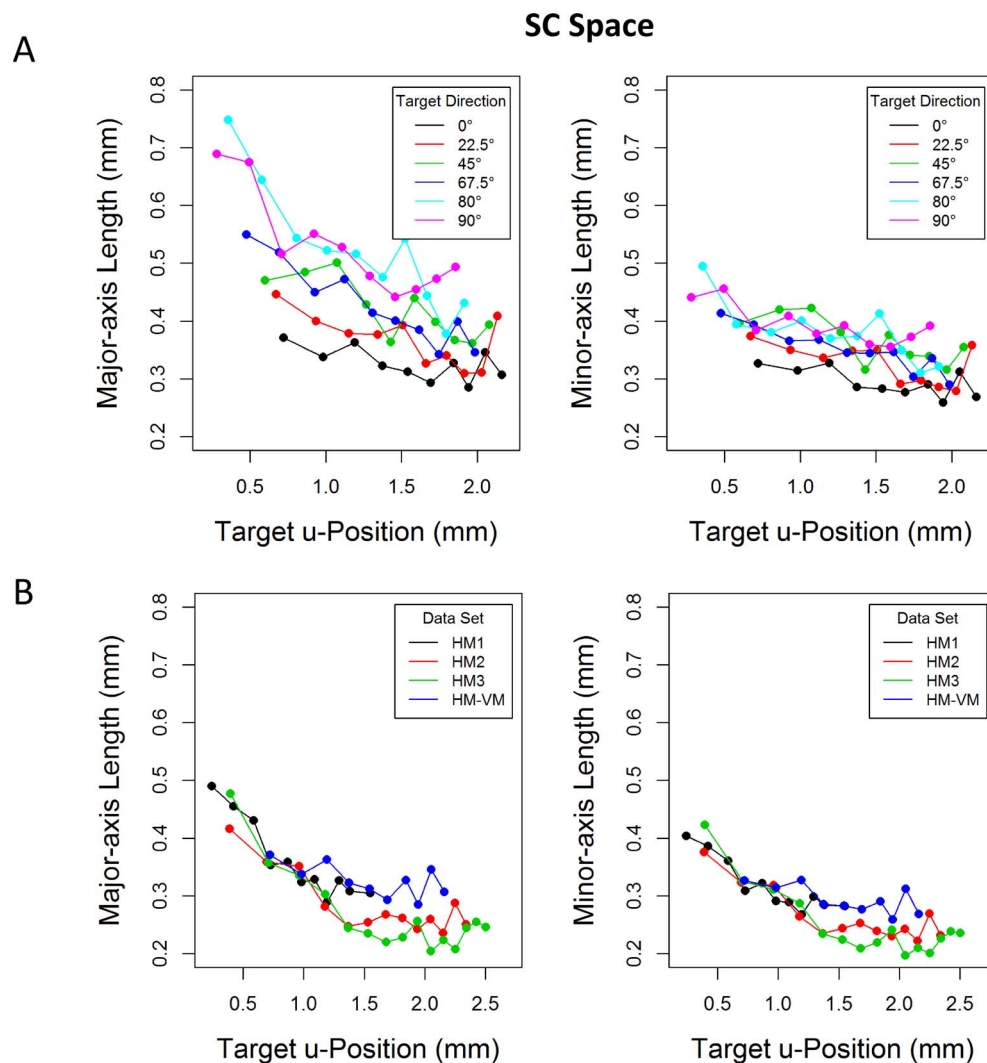


Figure 8. Mean length of major (left panels) and minor (right panels) axes of the ellipses fitted to 90%-isoline clusters of landing positions, expressed in millimeters of SC space, as a function of the target u -coordinate (along the rostrocaudal axis) in SC space (in millimeters) and target direction (in degrees; different colors) in the HM-VM data set (A), and as a function of the target u -coordinate (in millimeters) in HM1 (black), HM2 (red), and HM3 (green) data sets, as well as in the horizontal condition of HM-VM (blue) (B).

may contribute as well. However, this can also not be the only explanation because bilateral landing position distributions were observed mainly in the 90° condition.

In summary, as predicted by the MF account, and in contradiction to the downstream gain-adjustment hypothesis, the spread of saccadic endpoints increased with target eccentricity in visual space, but not in SC space. Yet the eccentricity-related increase in visual space was slower within, compared with outside, an extended, 5°, foveal region and slower than predicted by nonhomogeneous efferent mapping. Correspondingly, the variability in SC space, otherwise invariant, increased as the target moved from an eccentricity of about 5° to near the center of the fovea and even more so as it was displayed closer to the vertical meridian.

The shape of landing-position distributions

In line with the anisotropic representation of visual space, we observed that probability density functions formed elongated areas along the eccentricity axis in visual space but tended to be rounded in shape in SC space, at least for targets displayed outside an extended foveal region and away from the vertical meridian (see Figures 2–4). To further assess the elliptic versus circular shape of visual and collicular distributions, we computed the ratio between the lengths of major and minor ellipse axes. As expected, the ratio was significantly greater than 1 in visual space but very close to 1 in SC space (intercept estimates: 1.136 vs. 1.115, 1.184 vs. 1.052, 1.200 vs. 1.044, and 1.226 vs. 1.027 in HM1, HM2, HM3, and HM-VM, respectively), although still

significantly different from 1 in all data sets but HM-VM (see Appendix 1, Table A4A–B).

Furthermore, as shown in the left panels of Figure 9A–B, the ratio in visual space increased with target eccentricity, as assessed by the significant linear effect of eccentricity (and the positive slope) in all data sets, except HM1 (estimates: 0.026, 0.020, and 0.037 in HM2, HM3, and HM-VM, respectively; see Appendix 1, Table A4A; but see van Opstal & van Gisbergen, 1989b). It also tended to be slightly greater on and near the vertical meridian (80° and 90° axes), as suggested by the significant effect of target direction in the HM-VM data set (estimate: 0.002). In SC space, to the contrary, the ratio remained invariant toward the periphery but increased toward the representation of an extended foveal region (0.5° – 5°) and even more so when moving from the 45° to the 90° axis representation (see right panels of Figure 9A–B). In all data sets, the quadratic component of the effect of eccentricity was significant (estimates: 0.005, 0.001, 0.001, and 0.003 in HM1, HM2, HM3, and HM-VM, respectively; see Appendix 1, Table A4B), and there was a significant linear, negative trend in HM1 and HM3 (estimates: -0.028 and -0.003 , respectively); the slope was still larger in HM1, where the range of target eccentricities was smaller (0.5° – 6°), and the linear trend in visual space was nonsignificant (see above). In the HM-VM data set, the effect of direction and the interaction between direction and the linear eccentricity component were also significant (estimates: 0.003 and -0.0004 , respectively).

We noted above that variations in the spread of landing positions in SC space across data sets and target directions were in part due to differences in the target's u -coordinate on the rostrocaudal axis. In Figure 9C, the ratio of major-to-minor axis length in SC space was thus replotted as a function of the target's u -coordinate in HM-VM and HM data sets (left and right panels, respectively). This indicates that landing-position distributions tended to be relatively circular (ratio only slightly greater than 1) when targets were projected further than about 1 mm from the rostral pole. For targets projected within less than 1 mm, the distributions were more like ellipses that were gradually more elongated as targets projected closer to the rostral pole but still more so closer to the representation of the vertical meridian. Thus, the target's coordinate on the rostrocaudal axis seemed to play a role, but again could not be the only explanation for the effect of target direction. Similarly, the fact that landing-position distributions tended to be bilateral for small-amplitude saccades along the 90° , and to some extent the 80° , axis, although likely contributing, could not account by itself for the remaining differences as a function of target direction, because these ranged from the oblique to the vertical conditions.

In sum, as expected from both the anisotropic representation of visual space in the SC and the MF, landing-position distributions in visual space formed ellipses, which were further elongated along the eccentricity axis as the target was more peripheral, but they formed relatively circular-invariant areas in SC space. Yet as the target entered an extended foveal region, and even more so as it moved from the oblique to the vertical axis, landing-position clusters in SC space became gradually more elliptic in shape.

The (a-)symmetry of landing-position distributions

Following van Opstal and van Gisbergen (1989b), we initially assumed that the location of point images may be subject to rotation-symmetrical Gaussian variations. Given nonhomogeneous efferent mapping, these variations should yield landing-position distributions that are skewed away from the fovea, exactly as circularly symmetric population activity in the SC converts into positively skewed response fields (Ottes et al., 1986; see also Sparks et al., 1976; van Opstal et al., 1990). Yet, as suggested by previous behavioral studies, the distributions of saccadic endpoints tend to be biased toward, and not away from, the fovea (Lemij & Collewijn, 1989; van Opstal & van Gisbergen, 1989b). Here, we thus reexamined this issue further by estimating both the absolute asymmetry and the signed skewness of the probability density functions of landing positions along eccentricity/ u and direction/ v axes in visual and SC spaces.

As shown in the left panels of Figure 10A–B, all landing-position distributions in visual space exhibited an asymmetry that increased gradually with target eccentricity and to about the same extent for all target directions, as further suggested by HM-VM data. Accordingly, LME analyses revealed that the intercept estimate for the asymmetry index was significantly different from zero in all data sets (0.028, 0.077, 0.058, and 0.143, in HM1, HM2, HM3, and HM-VM, respectively; see Appendix 1, Table A5A). Furthermore, the linear effect of target eccentricity was significant in HM2, HM3, and HM-VM data sets (estimates: 0.010, 0.012, and 0.022, respectively), whereas in HM1, the quadratic effect of target eccentricity was significant (estimate: 0.004); the interaction between target eccentricity and direction in HM-VM was not significant. As further revealed in Tables A6A–A7A of Appendix 1, the asymmetry in visual space mainly came from negative skewness along the eccentricity axis, which is amplitude skewness toward the fovea. In HM2, HM3, and HM-VM, the intercept estimate for amplitude skewness was negative and significantly different from zero (-0.030 , -0.042 ,

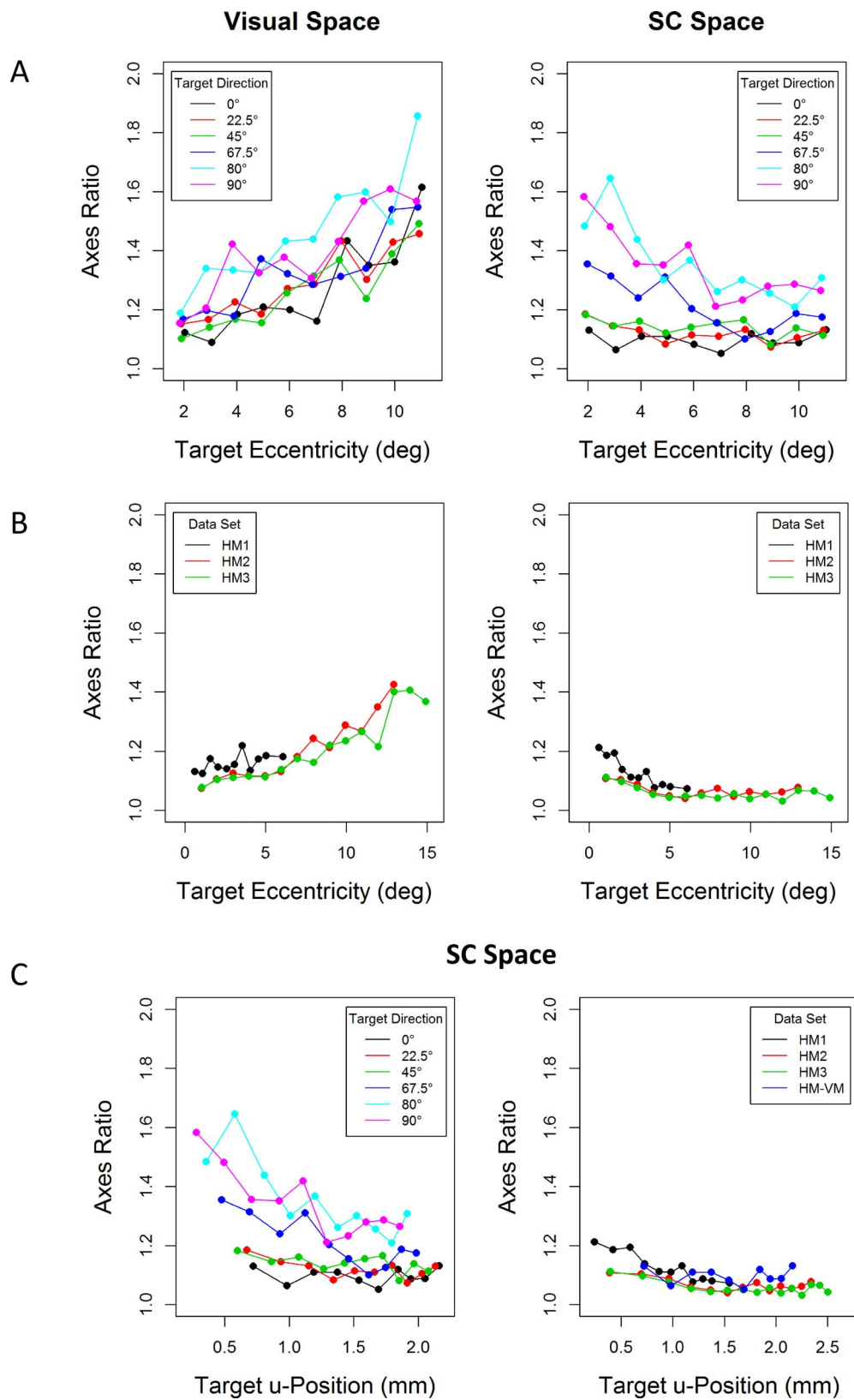


Figure 9. Mean ratio of major-to-minor-axis length of the fitted ellipses in visual (left panels) and SC space (right panels) as a function of target eccentricity (in degrees) and target direction (in degrees; different colors) in the HM-VM data set (A) and as a function of target eccentricity (in degrees) in HM1 (black), HM2 (red), and HM3 (green) data sets (B). In (C), mean ratios were replotted as a function of the target *u*-coordinate (along the rostrocaudal axis) in SC space (in millimeters) in HM-VM (left panel) and in HM1, HM2, and HM3 data sets, as well as in the horizontal condition of HM-VM (blue; right panel).

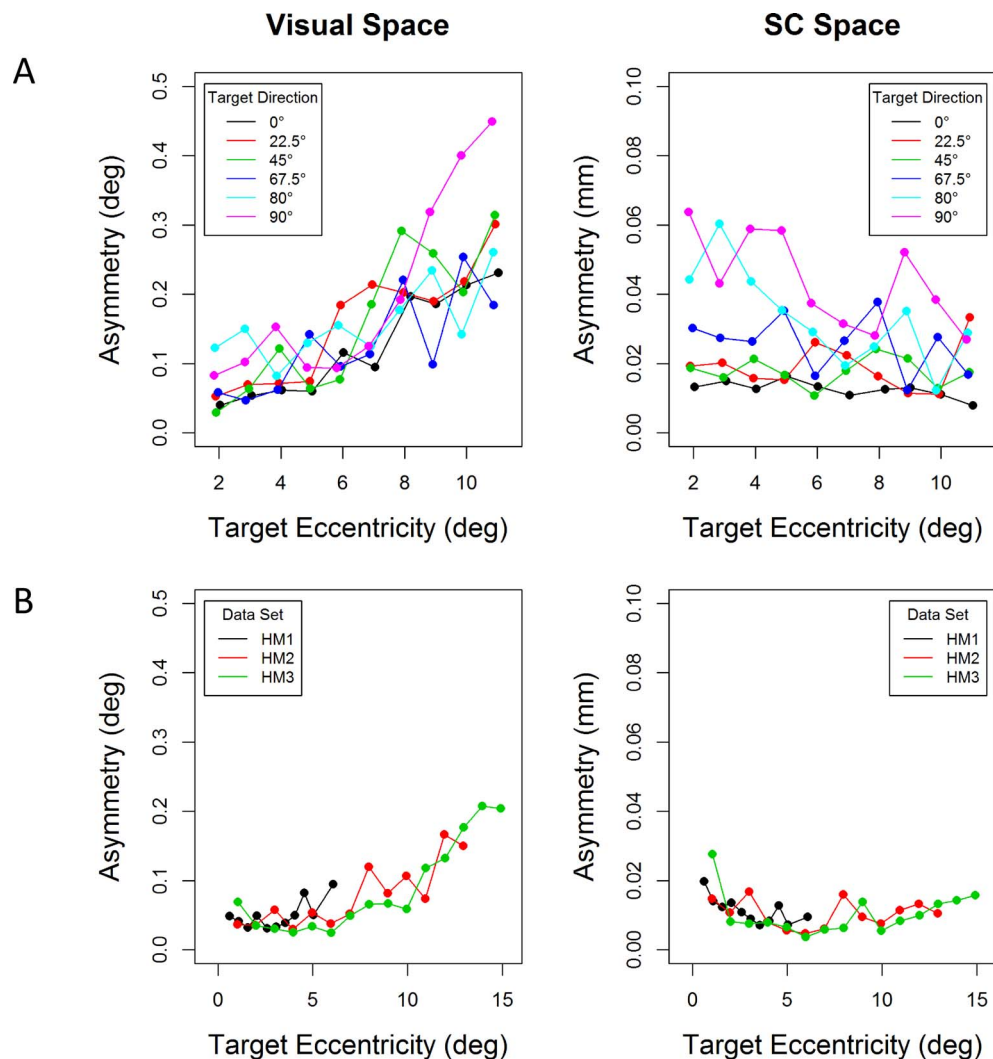


Figure 10. Mean estimated asymmetry (see the Methods section) of two-dimensional probability density functions of initial landing positions in degrees of visual angle (left panels) and millimeters of SC space (right panels) as a function of target eccentricity (in degrees) and target direction (in degrees; different colors) in the HM-VM data set (A) and as a function of target eccentricity (in degrees) in HM1 (black), HM2 (red), and HM3 (green) data sets (B).

and -0.047 , respectively), whereas that for direction skewness was never significant. Furthermore, similar to the asymmetry index, the amplitude skewness increased linearly with target eccentricity in all data sets, except HM-VM (estimates: -0.008 , -0.006 , and -0.012 in HM1, HM2, and HM3 data sets). In HM-VM, only the effect of target direction was significant (estimate: 0.001); the positive slope indicated that the negative bias reduced as the target moved from the horizontal to the vertical meridian.

In SC space, landing-position distributions were also significantly asymmetric in all data sets (intercept estimates: 0.009 , 0.010 , 0.007 , and 0.010 in HM1, HM2, HM3, and HM-VM, respectively; see Appendix 1, Table A5B). Still, as further illustrated in the right panels of Figure 10A–B, the asymmetry remained unaffected by target eccentricity, except for targets

displayed within less than 45° from the vertical meridian in HM-VM and also toward the fovea, as further suggested by HM data. In these particular conditions, the asymmetry was increased, yielding in turn a significant interaction between eccentricity and direction (estimate: -0.00004) and a significant effect of direction (estimate: 0.0003) in HM-VM, as well as significant linear and quadratic effects of eccentricity in HM1 (estimates: -0.002 and 0.0007 , respectively); note that the latter, linear, trend was negative, thus indicating an increasingly greater asymmetry toward the representation of the fovea. As in the case of the asymmetry in visual space, the asymmetry in SC space mainly came from negative skewness along the eccentricity, u -axis (see Appendix 1, Tables A6B–A7B). The negative intercept estimate for amplitude skewness was significantly different from zero in all data sets

except HM1 (−0.003, −0.006, and −0.006 in HM2, HM3, and HM-VM, respectively), whereas that for direction skewness was significant only in HM-VM (estimate: 0.002). Amplitude skewness showed no significant variation with eccentricity except in HM3, where both the linear and the quadratic components were significant (estimates: −0.001 and 0.0001, respectively). In HM-VM, there was an interaction between eccentricity and direction (estimate: −0.00004).

In sum, landing-position distributions in visual space were asymmetric and skewed toward the fovea but progressively more as the target was further out in the periphery and also closer to the horizontal meridian (see also Lemij & Collewijn, 1989; but see van Opstal & van Gisbergen, 1989b). Likewise, corresponding distributions in SC space were not symmetric but negatively biased along the u -axis. Yet, this asymmetry was relatively invariant across eccentricities, except again near the foveal and vertical-meridian representations in some data sets. Thus, the peripheral increase in visual negative skewness could be explained by nonhomogeneous efferent mapping, but negative skewness itself cannot. Negative skewness is also not consistent with our initial assumption that jitter in the location of point images is rotation symmetrical.

The mode of landing-position distributions: The systematic undershoot error

In line with previous studies, our data revealed a systematic undershoot tendency in visual space: Landing-position distributions systematically peaked in front of the target, with this effect increasing as the target appeared further in the periphery (Figures 2A and 3A). This is further illustrated in the left panels of Figure 11A–B, where the mean landing-position error along the eccentricity axis in visual space was plotted as a function of target eccentricity and direction in HM-VM and target eccentricity in HM data sets. In all data sets, and irrespective of target direction in HM-VM, the negative landing-position error increased gradually as the target became more eccentric. As revealed by LME analyses, the intercept estimate was small but significantly different from zero (−0.140, −0.207, −0.129, and −0.374 in HM1, HM2, HM3, and HM-VM, respectively; see Appendix 1, Table A8A). Furthermore, as predicted by both MF and gain-adjustment hypotheses, the relationship with eccentricity was linear, as assessed by the significant negative slope in all data sets (estimates: −0.030, −0.026, −0.026, and −0.057 in HM1, HM2, HM3, and HM-VM, respectively). Yet the trend was also quadratic in HM3 (estimate: −0.002); this was the result of a slower increase for targets falling within, compared with outside, the extended foveal region. Furthermore, as suggested by the significant

interaction between target eccentricity and direction in HM-VM (estimate: −0.0005), the linear relationship became slightly stronger as the target appeared closer to the vertical meridian.

The corresponding amplitude gain was greater than in several previous studies (>0.9), but it still differed significantly from 1 in all data sets (intercept estimate [p value]: 0.953 [0.0007], 0.983 [0.0431], 0.989 [0.0004], and 0.950 [0.0050] in HM1, HM2, HM3, and HM-VM, respectively). It overall remained unaffected by target eccentricity; only the quadratic effect of eccentricity in HM2 (slope estimate: −0.00113, $p = 0.0000$) and the interactions between eccentricity and direction in HM-VM were significant (slope estimates: −0.00011, $p = 0.0001$, and 0.00002, $p = 0.0433$, for Eccentricity \times Direction and Eccentricity² \times Direction, respectively).

In SC space, the landing-position error was again negative and significantly different from zero (intercept estimates: −0.030, −0.031, −0.028, and −0.049 in HM1, HM2, HM3, and HM-VM, respectively; see Appendix 1, Table A8B). However, and consistent with the MF account, the relationship with target eccentricity was nonsignificant in all data sets (see also right panels of Figure 11A–B). Still, as observed in visual space, the amplitude error in SC space tended to become smaller at small eccentricities (2°–4°) and greater at large eccentricities, as the target appeared closer to the vertical meridian; the interaction between eccentricity and direction in HM-VM was again significant (estimate: −0.00007).

In sum, there was a systematic saccadic undershoot in visual space, which increased linearly as the target moved from nearly the center of the fovea to a 15° peripheral location. In SC space, thus when landing positions were log-scaled according to the MF, the undershoot error was maintained, but it no longer varied with target eccentricity, therefore suggesting that the undershoot is already implemented in the SC or upstream, rather than originating from downstream.

Latency-based analyses of landing-position distributions

Previous studies reported that the latency of saccades to single targets remains relatively unaffected by target eccentricity, although being systematically longer for targets displayed within the foveal region and to some extent in the far periphery ($\geq 20^\circ$; e.g., Kalesnykas & Hallett, 1994). As shown in Table 1, the present data exhibited a similar pattern (see also Casteau & Vitu, 2012). Along the horizontal meridian, saccade latency remained invariant for stimuli displayed at eccentricities ranging between about 4° and 10° but gradually increased as the target appeared closer to fixation and to a smaller extent further than 10°. On other target

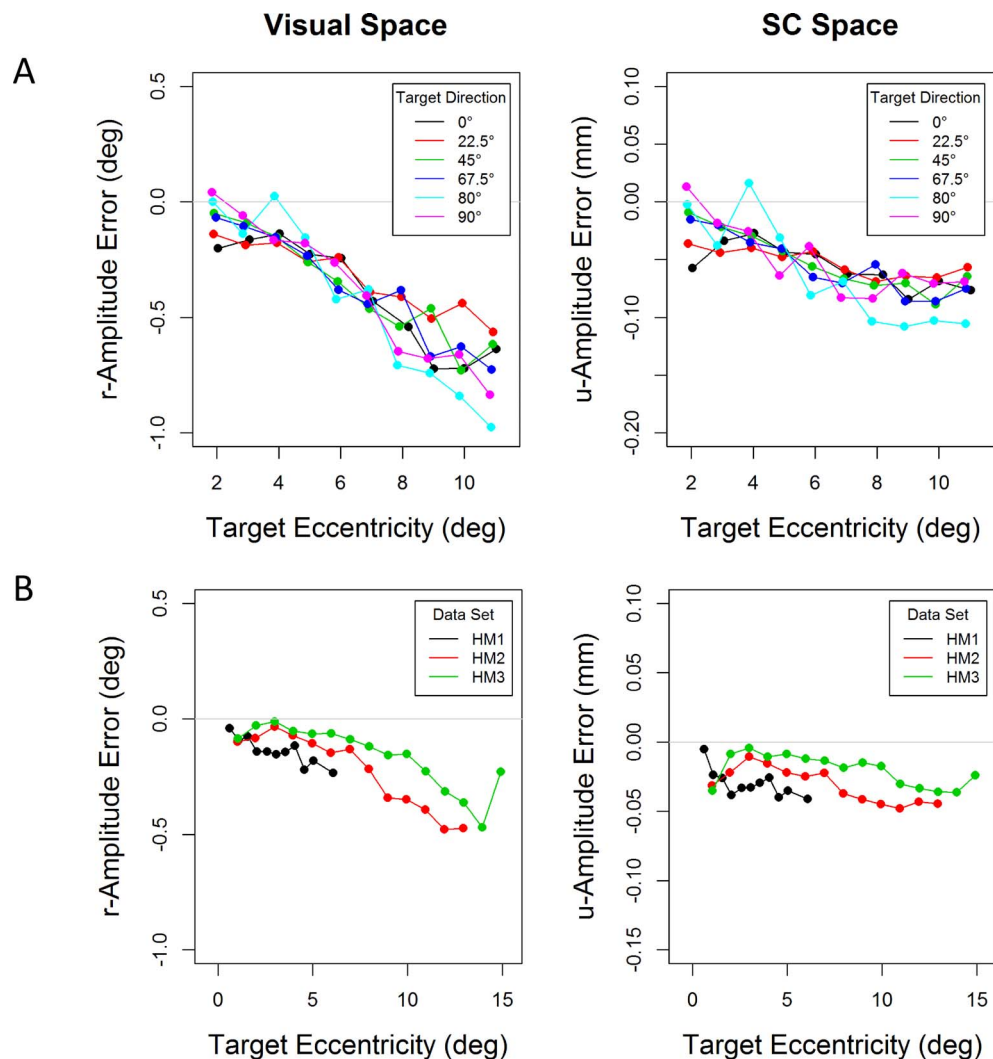


Figure 11. Mean radial- and u -amplitude errors of initial landing positions expressed, respectively, in degrees of visual angle (left panels) and millimeters of SC space (right panels) as a function of target eccentricity (in degrees) and target direction (in degrees; different colors) in the HM-VM data set (A) and as a function of target eccentricity (in degrees) in HM1 (black), HM2 (red), and HM3 (green) data sets (B). Zero values corresponded to perfectly accurate saccades, and negative values corresponded to an undershoot, or bias toward the (representation of the) fovea.

axes, the pattern was similar, with saccade latency increasing below 4° – 5° and above 8° – 9° , depending on target direction. As summarized in Table A9 of Appendix 1, there was a significant quadratic effect of target eccentricity in all data sets (estimates: 3.654, 0.680, 0.536, and 0.405 in HM1, HM2, HM3, and HM-VM, respectively), as well as a significant, negative, linear trend in HM1 (estimate: -5.500); the effect of target direction in HM-VM was also significant (estimate: -0.109), although revealing no consistent pattern from the horizontal to the vertical meridian.

These variations in saccade latency over the tested range of target eccentricities and directions raise the question of whether the above-reported properties of landing-position distributions were not the by-product of differences in saccade latency. To investigate this

issue, the bivariate probability density functions of landing positions in visual and SC spaces as well as corresponding isolines were recomputed after splitting the data for each individual, condition, and data set, in two equal saccade-latency bins; note that this forced us to use a slightly greater bandwidth (0.4° and 0.04 mm instead of 0.3° and 0.02 mm, respectively). The first bin comprised saccades that were launched with a latency equal to or less than the median latency in a given condition and individual, whereas the second comprised the remaining saccades. LME analyses were conducted using the two most diagnostic distribution indexes as dependent variables: the area subtended by 90% isolines and the amplitude error. The same top-down procedure used in the above analyses was adopted to determine the optimal random and fixed

Eccentricity	HM1 0°	HM2 0°	HM3 0°	HM-VM 0°	HM-VM 22.5°	HM-VM 45°	HM-VM 67.5°	HM-VM 80°	HM-VM 90°
0.5°	250								
1°	204	215	214						
1.5°	188								
2°	185	180	182	182	184	181	178	173	176
2.5°	182								
3°	186	169	175	177	172	171	172	168	169
3.5°	190								
4°	189	168	170	170	173	172	167	165	169
4.5°	186								
5°	187	167	172	169	172	170	161	163	168
6°	191	167	171	167	167	170	160	161	165
7°		169	170	172	173	167	159	158	166
8°		166	168	171	173	172	168	162	169
9°		168	171	171	181	172	163	160	165
10°		169	169	174	183	175	162	164	167
11°		171	172	169	186	176	166	164	171
12°		172	175						
13°		177	176						
14°			179						
15°			186						

Table 1. Mean saccade latency (in ms) as a function of eccentricity, and eccentricity and direction, in HM and HM-VM data sets respectively.

structures (see the Methods section). The initial fixed structure comprised, in addition to the above effects, the effect of saccade latency and its interaction with all other predictors (i.e., both the linear and quadratic components of the effect of target eccentricity in HM data sets as well as the [linear] effect of target direction in HM-VM), thus including not only two- but also three-way interactions in that particular data set. The latency variable corresponded to the bin number, which was entered as a categorical predictor with two levels (1 and 2).

The above analyses revealed that the spread of landing positions in visual space increased gradually with target eccentricity, although at a smaller rate within an extended foveal region of about 5°. As shown in Figure 12 (left panels) and Table A10A of Appendix 1, this held true when data were split by saccade latency. In all data sets, there was a positive linear relationship between the area subtended by 90% isolines and target eccentricity in the first, short-latency, bin (estimates: 0.196, 0.265, 0.223, and 0.246 in HM1, HM2, HM3, and HM-VM, respectively). Furthermore, in HM2 and HM3 data sets where the range of target eccentricities was the largest, the quadratic component of the effect of eccentricity was also significant, indicating again a slower increase of landing-position scatter within about 5° from the center of the fovea (estimates: 0.013 and 0.017, respectively). Importantly, as saccade latency increased, landing

positions were less widely spread, as assessed by the significant effect of bin in all data sets (estimates: -0.264 , -0.393 , -0.699 , and -0.209 , in HM1, HM2, HM3, and HM-VM, respectively). The relationship between spread and eccentricity was also weaker for longer-latency saccades in HM2 and HM3, as suggested by the interaction between bin and the linear component of the effect of eccentricity (estimates: -0.088 and -0.055 , respectively), but the effect of eccentricity remained significant (estimates: 0.1771, $p < 0.0000$ and 0.1680, $p < 0.0000$, respectively). Yet the interaction between bin and the quadratic component of the effect of eccentricity was not significant in these two data sets, and none of the interactions were significant in HM1, where eccentricities ranged between 0.5° and 6°. This suggests that the slower eccentricity-related increase in spread within, compared with outside, the extended foveal region was not due to small-amplitude saccades being launched with longer latencies.

We reported above that the distributions of landing positions in visual space peaked in front of the target, and proportionally more as the target was displayed further out in the periphery, and even more so closer to the vertical meridian. The present time-based analyses of the amplitude error revealed that this was maintained in the first latency bin, thus when saccade latencies were shorter (see Figure 12, right panels). The undershoot error was significant again in all data sets

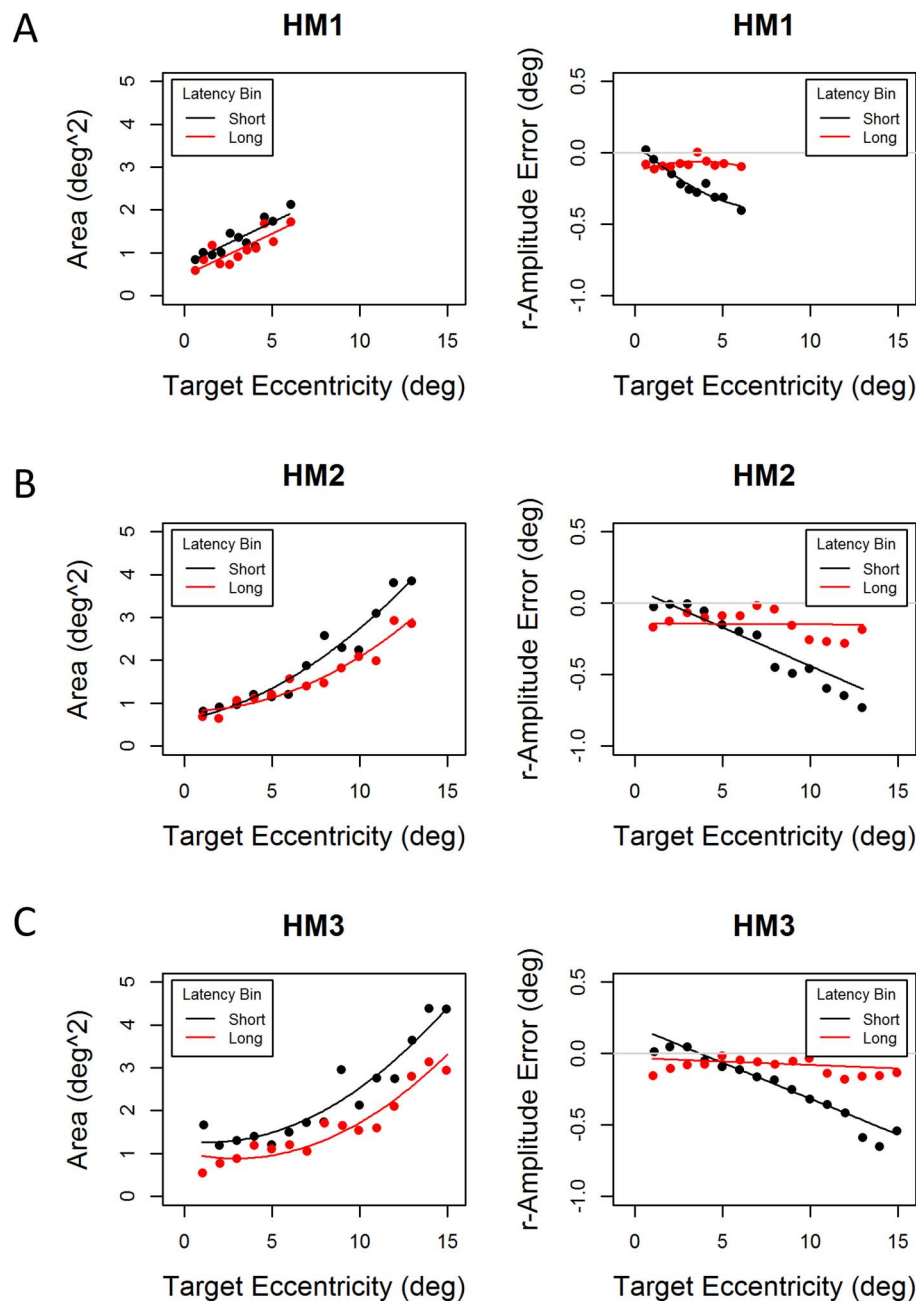


Figure 12. Mean area subtended by 90%-isoline clusters of landing positions (left panels) and mean amplitude error (right panels) in visual space as a function of target eccentricity (in degrees) and for two equal bins of saccade latencies (short latency: black; long latency: red) in HM1 (A), HM2 (B), and HM3 (C) data sets. Lines corresponded to the curves estimated by corresponding LME models.

(intercept estimates: -0.225 , -0.276 , -0.214 , and -0.439 in HM1, HM2, HM3, and HM-VM, respectively; see Appendix 1, Table A10B), and it increased linearly with target eccentricity, as assessed by the significant negative slope estimates (-0.072 , -0.054 , -0.050 , and -0.083 in HM1, HM2, HM3, and HM-VM, respectively). It was also more pronounced as the target appeared closer to the vertical meridian, as suggested by the significant interaction between eccentricity and direction in HM-VM (estimate: -0.0004). These results suggest that the undershoot phenomenon

and its relationship with eccentricity and direction are not due to differences in saccade latency. Still, in all data sets but HM-VM, there was a significant effect of bin (estimates: 0.163 , 0.130 , and 0.144 in HM1, HM2, and HM3, respectively), which indicated that the undershoot error was overall reduced for longer-latency saccades; actually, this remained significant only in HM2 and HM-VM (estimates: -0.146 and -0.372 , respectively). Furthermore, the undershoot error no longer varied significantly with eccentricity (all p s ≥ 0.0683); the interaction between bin and the linear

component of the effect of eccentricity was significant in all data sets (estimates: 0.078, 0.053, 0.045, and 0.040 in HM1, HM2, HM3, and HM-VM, respectively), and the interaction between bin and the quadratic component of the effect of eccentricity was significant in HM1 (estimate: -0.013). This finding, which corroborates previous reports showing a reduction over time of the linear relationship between saccades' hypometria and target eccentricity (de Bie et al., 1987), further argues against an overall gain-adjustment account of the undershoot phenomenon, as further discussed below.

In summary, saccade latency had an impact on landing-position distributions. Delayed saccade onset reduced the spread, but it did not seem to be responsible for the slower eccentricity-related increase within, compared with outside, an extended foveal region. It also yielded greater accuracy, mainly to the benefit of peripheral targets, thereby reducing the effect of eccentricity on hypometria.

Discussion

As consistently shown in previous studies, saccadic eye movements tend to systematically undershoot an eccentric visual target, by about 10% of its eccentricity, while becoming proportionally more variable, mainly in amplitude, as the target appears further out in the periphery (Becker & Fuchs, 1969; Deubel, 1987; Frost & Pöppel, 1976). Across four parametric human eye-movement data sets, we first showed that these relationships generalize to visual targets displayed at eccentricities ranging between 0.5° and 15° along a range of axes, from the horizontal to the vertical meridian; yet we found that the eccentricity-related increase in variability was slower within, compared with outside, an extended foveal region of about 5° , and this across a range of saccade latencies. Second, we clearly established the fact, reported in a few previous studies only, that landing-position distributions are not only shifted but also consistently skewed toward the fovea, and to greater extents as the target is more peripheral (Lemij & Collewijn, 1989; see also van Opstal & van Gisbergen, 1989b). Third, and most important, our analyses revealed that when landing positions were log transformed, and the MF was taken into account, their distributions still exhibited a negative peak offset and asymmetry, but that no longer varied with eccentricity. Furthermore, the spread of saccadic endpoints was invariant in size and shape (i.e., almost perfectly circular) across a wide range of locations, although being increasingly larger and more elliptic in shape as the target entered again a 5° , foveal region, and even more so closer to the vertical meridian.

As further developed below, these findings suggest that the systematic undershoot, and corresponding variability, originate, in, or upstream of, the SC, rather than being the result of an overall adjustment of the gain of saccades downstream of the SC (Harris, 1995; see also Becker, 1989). The possibility, suggested by our data, but still in contradiction with our initial assumption, that the underlying location jitter in point images may neither be normally distributed nor invariant in size and shape across the entire visual-field representation, is discussed in relation with the properties of spatial coding in the brain.

Role of the MF: Evidence against a downstream account of hypometria and imprecision

It has long been thought that the systematic undershoot is a strategy that aims at avoiding landing past the target (Deubel et al., 1986; Henson, 1978). In line with this assumption, Harris (1995) proposed that the strategy is implemented downstream of the SC and consists of adjusting the gain of desired saccade amplitudes and correspondingly constraining their variability (see also Becker, 1989). According to his hypothesis, both the variability and the hypometria of saccades should increase linearly with eccentricity, with the standard deviation of landing-position errors being proportional to the average magnitude of the distance traveled. In line with these predictions, we found that landing-position distributions peaked in front of the target and that both their negative peak offset and their spread increased as the target moved from near the center of the fovea to an eccentricity of 11° – 15° , and this regardless of target direction. Although, just as predicted, the relationship between eccentricity and hypometria was linear, at least in three of four data sets, the eccentricity-related increase in variability was consistently slower within, compared with outside, an extended 5° foveal region. This is a novel finding that was not previously reported, in part because former studies did not manipulate target eccentricity in a parametric manner over the full range of ordinary saccade amplitudes. It reveals, in contradiction with Harris's (1995) hypothesis, that the variability in saccade amplitudes is not a constant proportion of the mean distance traveled (see also de Bie et al., 1987).

Another novel, and actually even more striking, finding is that neither the undershoot error nor the spread of the distributions increased with eccentricity, when landing positions were log-transformed and expressed in millimeters of SC space, thus taking the MF into account. From rostral to caudal, landing-position distributions peaked at a constant distance from the target location, meaning therefore that the observed pattern in visual space could be predicted by

the MF, assuming a constant error in SC space. Furthermore, although the spread gradually increased as the target moved from an eccentricity of about 5° to near the center of the fovea, and even more so closer to the vertical meridian, this was still invariant over the remaining set of target locations, that is, over the vast majority of tested locations. As there is no topographic and fovea-magnified representation of visual/motor space downstream of the SC, these findings clearly suggest that both the hypometria and the imprecision of saccades are already represented in, or upstream of, the SC. Therefore, they do not form downstream, that is after the target has been selected and the desired movement amplitude has been computed, as originally proposed by Harris (1995).

Evidence against a downstream locus of saccadic undershoot was never reported, but such evidence for saccade-endpoint scatter was originally provided by Deubel (1987). He reported that the variability of saccade endpoints is greater along than perpendicular to the eccentricity axis and argued that it is therefore likely represented in the polar coordinate system of the SC, rather than originating from downstream, where the horizontal and vertical components of saccades are coded independently. Van Opstal and van Gisbergen (1989b) replicated Deubel's (1987) findings and further argued that the elliptic shape of landing-position distributions might reflect the anisotropic representation of visual space in the SC, that is, the fact that it is more expanded along the direction, compared with the eccentricity, axis. In line with this suggestion, they reported the data of one participant, whose saccade endpoints, when replotted in SC space, formed roughly circular areas. Our results further corroborated their findings by showing across four data sets and a larger set of target locations, that bivariate probability density functions, and corresponding 90% isolines, formed ellipses in visual space but nearly circular areas in SC space. The only exception was again within the representation of an extended foveal region of about 5°, where the distributions were more elliptical in shape; note that the one-participant scatter plot in van Opstal and van Gisbergen's (1989b) article actually suggested the same trends for target eccentricities of 2° and 5° compared with more peripheral target locations.

Our additional observation that landing-position distributions in visual space were skewed toward the fovea (see also Lemij & Collewijn, 1989; van Opstal & van Gisbergen, 1989b), and hence only along the eccentricity axis, although being in contradiction with Harris's (1995) hypothesis that landing positions are normally distributed, is no argument for a SC representation of the variability. Indeed, corresponding distributions in SC space were also negatively skewed. However, the fact that negative skewness increased with eccentricity in visual but not in SC space is one

more piece of evidence against a downstream locus of the variability (for an alternative, although inconsistent, interpretation of negative skewness, see van Opstal & van Gisbergen, 1989b). Whether negative skewness relates to the systematic undershoot as revealed by the negative peak offset of saccade-endpoint scatter cannot be determined with the present data. Still, the fact that the two phenomena co-occur; that they both show a bias in the same, foveal, direction; and that they are both likely represented in the SC (or upstream) may suggest that they reflect the same underlying neural mechanisms, as further discussed below.

Our conclusion that the hypometria may already be represented in, or upstream of, the SC still remains controversial, particularly in light of Henson's (1978) original finding, that when the undershoot that normally occurs is compensated for by an experimentally induced shift of the saccade goal, it is restored very rapidly, after an adaptation period of a few minutes only (see also Deubel et al., 1986). Indeed, as suggested by a number of neural and behavioral studies, saccadic adaptation would more likely operate downstream of the SC, rather than in the SC (Fitzgibbon, Goldberg, & Seagraves, 1986; Frens & van Opstal, 1997; but see Takeichi, Kaneko, & Fuchs, 2007; for a review, see Pélisson, Alahyane, Panouillères, & Tilikete, 2010). One alternative explanation might be that saccadic adaptation, once established, leads to a systematic shift of the saccadic goal, either through projections to the SC or remapping of SC space. This would in turn allow a systematic undershoot of the saccadic goal to exhibit again, but then now because it is an inevitable property of the oculomotor system rather than an intended strategy.

The origin of hypometria and imprecision: Contrasting SC and upstream accounts

We used a model of the SC to test our hypothesis that the eccentricity-related increase in saccades' hypometria and imprecision comes from the MF in the brain. We had two main reasons for preferring a SC-modeling approach. First, despite the fact that many brain areas are devoted to visual processing, as well as the selection of a saccade target, the visuomotor transform necessary for a saccade command ultimately takes place in the SC (e.g., White & Munoz, 2011). Not only does the SC integrate afferent projections from many visual cortical areas, but it seems to prevail over the FEF in driving the activity of motor neurons in the reticular formation, even despite direct FEF projections onto these saccade generators (e.g., Hanes & Wurtz, 2001). We thus reasoned that as long as systematic and random errors do not find their origin

downstream of the SC, they must be represented in the SC regardless of whether they initially form in the SC or upstream. Second, Ottes et al.'s (1986) model of saccade programming in the SC, and in particular its afferent/efferent mapping function, had been validated in many studies. These showed, in accordance with the model's predictions, that response-field images as well as reconstructed point images in the SC-coordinate system are of about the same size regardless of where the eyes move (Anderson et al., 1998; Goossens & van Opstal, 2006; Marino et al., 2008; McIlwain, 1975; Moschovakis et al., 2001; Munoz & Wurtz, 1995b; van Opstal et al., 1990). Furthermore, although Hafed and Chen (2016) recently reported systematic asymmetries in the representation of upper versus lower visual fields, their data invalidated neither Ottes et al.'s (1986) claim that point images are relatively invariant over the representation of a visual-field quadrant nor their estimate of the MF factor along the rostrocaudal, eccentricity (u), axis. Actually, when applying the correction they proposed for computation of the direction, v , parameter, we obtained data patterns that were nearly identical to those reported above (not shown here).

Still, one obvious limitation is that Ottes et al.'s (1986) model was fitted to electrophysiological data from monkeys, not to human behavioral data, as in our study. Yet, using this model remained the best possible way to test our hypothesis, given that no such comparable model and data are yet available for humans. Furthermore, the fact that our findings showed that systematic and random errors were translation invariant over much of the representation of a visual-field quadrant somehow cross-validated our approach. Two reasons make it implausible that our observation of gradually larger and more elongated saccade-endpoint distributions as the target entered an extended foveal region, and also as it got closer to the vertical meridian, was due to Ottes et al.'s (1986) anisotropic afferent-mapping function being suboptimal for humans and/or near the fovea and the vertical meridian. First, we observed a mirror-image pattern when landing positions were expressed in degrees of visual angle, that is, before they were log transformed with Ottes et al.'s (1986) function: The eccentricity-related increase in variability was slower within, compared with outside, the 5° extended foveal region and less than that predicted by the MF. Second, we found the same trends when an isotropic-mapping function was used to convert degrees of visual angle into millimeters of SC space (not shown here).

Another limitation of our study is that we did not record neuronal activity. We therefore cannot assert that we estimated the properties of spatial coding in the SC and not somewhere else, nor can we assert that random and systematic saccadic errors originated from

the SC and not from upstream areas. Actually, several of the visual cortical areas that project onto the SC contain a topographic and fovea-magnified representation of eccentricity that is comparable to that in the SC (see Ottes et al., 1986). This is the case in particular for the primary visual cortex (e.g., Schwartz, 1980; van Essen et al., 1984) and Areas V2–V4 (e.g., Harvey & Dumoulin, 2011), as well as the FEF (Bruce & Goldberg, 1985; Sommer & Wurtz, 2000). Because the FEF is involved in visual selection as well as saccade generation, it could potentially be the primary locus for the hypometria and imprecision of saccades. Yet, as suggested by several studies, there seems to be a dichotomy in the FEF between a lateral region mainly devoted to visual analysis and the coding of eccentricities below 15° and a medial, motor, region representing essentially the far periphery (Sommer & Wurtz, 2000). Not only is this inconsistent with the dissociation we observed in saccade-endpoint scatter between target eccentricities below and above about 5° , but it also does not fit with the fact that the linear, eccentricity-related, increase in hypometria extends largely beyond the 1° – 15° range of ordinary saccade amplitudes (e.g., 5° – 45° ; Frost & Pöppel, 1976). Furthermore, the FEF, unlike the SC, does not seem to contain a topographic representation of direction (Bruce, Goldberg, Bushnell, & Stanton, 1985; Sommer & Wurtz, 2000). This seems hard to reconcile with consistent variability in landing positions along amplitude- and direction-axis representations.

Area V1, which has been more extensively studied, does contain a topographic representation of eccentricity and direction that is similar to that in the SC (van Essen et al., 1984). Its spatial coding properties still differ from those of the SC, in that the eccentricity-related increase in the neurons' receptive fields is not perfectly inversely proportional to the cortical MF (for a review, see McIlwain, 1986). As a result, point images in V1 are not translation invariant (but see Hubel & Wiesel, 1974). Several authors reported that they increase systematically from the representation of the far periphery (50° – 80°) to the region corresponding to the center of the visual field (Dow, Snyder, Vautin, & Bauer, 1981; Gattass, Sousa, & Rosa, 1987). Others, such as van Essen et al. (1984), found an asymmetric V-shape function, indicating that a point stimulus activates an increasingly larger population of neurons as it moves from an eccentricity of about 5.5° to the center of the fovea (see also Harvey & Dumoulin, 2011) and also as it becomes more peripheral. Although this may suggest that the larger spread of landing positions within the representation of an extended, 5° , foveal region reflected the variability of population activity in V1, our finding of translation-invariant spread over much of the periphery's representation was unlikely the result of spatial coding in V1. Note, though, that SC point

images, although being relatively translation invariant, also tend to be larger near the representation of the fovea ($\leq 2.5^\circ$; Anderson et al., 1998; van Opstal et al., 1990; but see Marino et al., 2008). On the other hand, our observation of a constant hypometria in SC space across a range of target eccentricities from 0.5° to 15° seems hard to reconcile with the reported nonhomogeneity of point images in V1 across the entire visual-field representation. Thus, although visual information likely transited through V1 and other cortical areas before, and while, projecting onto the SC, the distributions of saccadic endpoints could a priori not fully result from the properties of spatial coding in V1.

Our hypothesis that the hypometria and imprecision of saccades may not originate in areas upstream of the SC is further supported by several behavioral findings suggesting that these errors are not the effect of high-level, perceptual and strategy-based, processes, and hence top-down projections to the SC. In the past, the possibility that the undershoot phenomenon may reflect perceptual constraints was considered in light of findings revealing a more pronounced undershoot for briefly presented visual targets (Aitsebaomo & Bedell, 1992; see also Lemij & Collewijn, 1989) and following shorter saccade latencies (de Bie et al., 1987). Yet, as saccadic performance was found to be much worse than perceptual localization judgments, this hypothesis was rejected, and an account in terms of sensory-motor constraints was preferred. On the other hand, the possibility that the undershoot phenomenon and related variability result from a strategy that would be either built in the SC or associated with top-down projections does not hold. Indeed, according to either of these scenarios, one would reasonably expect the bias to be relatively invariant and hence to correspond to a rather constant rostral bias of the population-activity profile not only across the entire SC motor map but also across trials and saccade latencies. Not only would it be the simplest strategy that would yield, given nonhomogeneous efferent mapping, an eccentricity-related increase in target undershoot as typically observed, but this would also be a way to not take into account the contingencies that might occur on any given trial, which is what a strategy is precisely for. However, the finding, which we replicated in all four data sets, that the undershoot, and related variability, becomes less as saccade latency increases is in contradiction with this prediction (de Bie et al., 1987). Thus, rather than being the effect of cortical, perceptual or strategy-based, processes, the hypometria and imprecision of saccades may in fact mainly be due to sensory-motor constraints associated with the properties of spatial coding in the SC.

Several electrophysiological findings support the hypothesis that the variability in saccadic endpoints finds its source, at least in part, in the SC. These

reveal that saccades evoked by focal electrical stimulation of the deeper SC are, just as visually guided saccades, variable, mainly in amplitude, but also in direction, and gradually more as the stimulation site is more caudal (van Opstal et al., 1990; see also Schiller & Stryker, 1972). Importantly, electrical saccades are also preceded by activity of a population of neurons, presumably as a result of the lateral spread of excitatory activity (McIlwain, 1982), combined with longer-range inhibition (e.g., Munoz & Istvan, 1998; see also van Opstal & van Gisbergen, 1989a; for a review, see Isa & Hall, 2009). Although this is consistent with our assumption that the variability in saccadic endpoints may reflect location jitter in SC point images (see also van Opstal & van Gisbergen, 1989b), it may suggest in addition that location jitter results, at least partly, from variations in the strength, the extent, and/or the distribution of lateral interactions. There is yet no direct evidence for this rather speculative hypothesis. Still, a few findings suggest that lateral interactions could possibly yield variability in the location of point images, which is both greater near the SC borders and overall rostrally biased, as would be expected based on the here-observed properties of landing-position distributions in SC space. First, excitatory, intercollicular, connections, which are likely involved in the generation of small-amplitude and vertical saccades, tend to be denser near the rostral one-fourth of the SC and the vertical-meridian representation (Behan & Kime, 1996; Takahashi, Sugiuchi, Izawa, & Shinoda, 2005; see also Infante & Leiva, 1986; Olivier, Porter, & May, 1998; Olivier, Corvisier, Pauluis, & Hardy, 2000; Paré & Guitton, 1994). Moreover, intracollicular inhibition in the intermediate SC seems to be mostly directed away from the rostral pole (Meredith & Ramoa, 1998; Munoz & Istvan, 1998; but see Bayguinov, Ghitani, Jackson, & Basso, 2015; Phongphanphane, Marino, Kaneda, Yanagawa, Munoz, & Isa, 2014).

Regardless of whether the horizontal SC circuitry may be involved, it is worth noting that population activity in buildup layers, contrary to that in burst layers, tends to be skewed, and also more variable, toward the rostral pole (Anderson et al., 1998; Munoz & Wurtz, 1995a, 1995b; see also Hafed & Chen, 2016; Marino et al., 2008; Nakahara, Morita, Wurtz, & Optican, 2006). Under the assumption that the eyes move to the location in space that corresponds to the weighted centroid of the active population (see Lee, Rohrer, & Sparks, 1988), this trial-by-trial rostral bias in the population-activity profile could possibly result in (across trials) landing-position distributions that are negatively skewed and also peak in front of the target. Whether this would be the explanation for the well-known, systematic undershoot phenomenon, and re-

lated variability, and more generally, whether both the hypometria and the imprecision of saccades originate in the SC or alternatively upstream of the SC, cannot, however, be firmly established at this stage. Further investigations are necessary that would optimally combine our parametric behavioral approach with electrophysiological recordings in the monkey to jointly estimate the accuracy of visually evoked saccades and the metrical properties of underlying population-activity profiles in different SC layers, as well as in visual cortical areas.

Conclusion

We found that the greater hypometria and imprecision of larger saccades can largely be accounted for by the MF in our brain. As there is no topographic and fovea-magnified representation of visual space downstream of the SC, our results provide a strong case against the classical, downstream, strategy-based account of the undershoot phenomenon and related variability. Our approach and findings also suggest that mapping saccadic endpoints into a log-space coordinate system allows the parceling out of variance attributable purely to properties of the SC and upstream cortical areas, in opposition with downstream structures, thereby offering new perspectives for a complete understanding of saccadic behavior.

Keywords: saccade-endpoint scatter, systematic undershoot, magnification factor, point image, superior colliculus

Acknowledgments

The present work was supported by a French-German ANR-DFG grant awarded to Françoise Vitu (ANR-10-FRAL-009-0; 2011-2014) and both a grant from the French Ministry of Research (“Allocation de recherche”; 2008–2011) and from the Fyssen Foundation (2013–2015) awarded to Soazig Casteau. It was presented in parts at VSS 2013, ECEM 2013 and 2015, and NCM 2014. We would like to thank Daniel Guitton for commenting on a previous version of this article.

Commercial relationships: none.

Corresponding author: Françoise Vitu.

Email: Francoise.Vitu-Thibault@univ-amu.fr.

Address: Laboratoire de Psychologie Cognitive, CNRS, Aix-Marseille Université, Marseille, France.

References

- Abrams, R. A., Meyer, D. E., & Kornblum, S. (1989). Speed and accuracy of saccadic eye movements: Characteristics of impulse variability in the oculomotor system. *Journal of Experimental Psychology: Human Perception and Performance*, *15*, 529–543.
- Aitsebaomo, A. P., & Bedell, H. E. (1992). Psychophysical and saccadic information about direction for briefly presented stimuli. *Vision Research*, *32*, 1729–1737.
- Anderson, R. W., Keller, E. L., Gandhi, N. J., & Das, S. (1998). Two-dimensional saccade-related population activity in superior colliculus in monkey. *Journal of Neurophysiology*, *80*, 798–817.
- Bahill, A. T., Adler, D., & Stark, L. (1975). Most naturally occurring saccades have magnitudes 15 degrees or less. *Investigative Ophthalmology & Visual Science*, *14*, 468–469. [PubMed] [Article]
- Bayguinov, P. O., Ghitani, N., Jackson, M. B., & Basso, M. A. (2015). A hard-wired priority map in the superior colliculus shaped by asymmetric inhibitory circuitry. *Journal of Neurophysiology*, *114*, 662–676.
- Behan, M., & Kime, N. M. (1996). Spatial distribution of tectotectal connections in the cat. *Progress in Brain Research*, *112*, 131–142.
- Becker, W. (1989). Metrics. In R. H. Wurtz & M. E. Goldberg (Eds.), *The neurobiology of saccadic eye movements* (pp. 13–67). Amsterdam: Elsevier.
- Becker, W., & Fuchs, A. F. (1969). Further properties of the human saccadic system: Eye movements and correction saccades with and without visual fixation points. *Vision Research*, *9*, 1247–1258.
- Bruce, C. J., & Goldberg, M. E. (1985). Primate frontal eye fields: I. Single neurons discharging before saccades. *Journal of Neurophysiology*, *53*, 603–635.
- Bruce, C. J., Goldberg, M. E., Bushnell, M. C., & Stanton, B. (1985). Primate frontal eye fields. II. Physiological and anatomical correlates of electrically evoked eye movements. *Journal of Neurophysiology*, *54*, 714–734.
- Casteau, S. (2012). Etude des mécanismes de génération des mouvements saccadiques chez l’homme: effets des propriétés de la configuration visuelle sur la latence et la métrique des saccades (unpublished doctoral dissertation). Université de Provence, France.
- Casteau, S., & Vitu, F. (2012). On the effect of remote and proximal distractors on saccadic behavior: A challenge to neural-field models. *Journal of Vision*,

- 12(12):14, 1–33, doi:10.1167/12.12.14. [PubMed] [Article]
- Castet, E., & Crossland, M. (2012). Quantifying eye stability during a fixation task: A review of definitions and methods. *Seeing and Perceiving*, 25, 449–469.
- Cynader, M., & Berman, N. (1972). Receptive-field organization of monkey superior colliculus. *Journal of Neurophysiology*, 35, 187–201.
- de Bie, J., van den Brink, G., & van Sinderen, J. (1987). The systematic undershoot of saccades: A localization or an oculomotor phenomenon? In J. K. O'Regan & A. Lévy-Schoen (Eds.), *Eye movements: From physiology to cognition* (pp. 85–94). New York: Elsevier.
- Deubel, H. (1987). Adaptivity of gain and direction in oblique saccades. In J. K. O'Regan & A. Lévy-Schoen (Eds.), *Eye movements: From physiology to cognition* (pp. 181–190). North Holland, the Netherlands: Elsevier Science.
- Deubel, H., Wolf, W., & Hauske, G. (1986). Adaptive gain control of saccadic eye movements. *Human Neurobiology*, 5, 245–253.
- Dow, B. M., Snyder, A. Z., Vautin, R. G., & Bauer, R. (1981). Magnification factor and receptive field size in foveal striate cortex of the monkey. *Experimental Brain Research*, 44, 213–228.
- Evdokimidis, I., Tsekou, H., Smyrnis, N. (2006). The mirror antisaccade task: Direction amplitude interaction and spatial accuracy characteristics. *Experimental Brain Research*, 174, 304–311.
- Findlay, J. M. (1982). Global visual processing for saccadic eye movements. *Vision Research*, 22, 1033–1045.
- Fitzgibbon, E. J., Goldberg, M. E., & Seagraves, M. A. (1986). Short term saccadic adaptation in the monkey. In E. S. Keller & D. S. Zee (Eds.), *Adaptive processes in visual and oculomotor systems* (pp. 329–333). Oxford, UK: Pergamon Press.
- Frens, M. A., & van Opstal, A. J. (1997). Monkey superior colliculus activity during short term saccadic adaptation. *Brain Research Bulletin*, 43, 473–483.
- Frost, D., & Pöppel, E. (1976). Different programming modes of human saccadic eye movements as a function of stimulus eccentricity: Indications of a functional subdivision of the visual field. *Biological Cybernetics*, 23, 39–48.
- Gattass, R., Sousa, A. P. B., & Rosa, M. G. P. (1987). Visual topography of V1 in the cebus monkey. *Journal of Comparative Neurology*, 259, 529–548.
- Gillen, C., Weiler, J., & Heath, M. (2013). Stimulus-driven saccades are characterized by an invariant undershooting bias: No evidence for a range effect. *Experimental Brain Research*, 230, 165–174.
- Girard, B., & Berthoz, A. (2005). From brainstem to cortex: Computational models of saccade generation circuitry. *Progress in Neurobiology*, 77, 215–251.
- Goffart, L. (2009). Saccadic eye movements. *Encyclopedia of Neuroscience*, 8, 437–444.
- Goldberg, M. E., & Wurtz, R. H. (1972). Activity of superior colliculus in behaving monkey: I. Visual receptive fields of single neurons. *Journal of Neurophysiology*, 35, 542–559.
- Goossens, H. H. L. M., & van Opstal, A. J. (2006). Dynamic ensemble coding of saccades in the monkey superior colliculus. *Journal of Neurophysiology*, 95, 2326–2341.
- Hafed, Z. M., & Chen, C.-Y. (2016). Sharper, stronger, faster upper visual field representation in primate superior colliculus. *Current Biology*, 26, 1647–1658.
- Hanes, D. P., & Wurtz, R. H. (2001). Interaction of the frontal eye field and superior colliculus for saccade generation. *Journal of Neurophysiology*, 85, 804–815.
- Harris, C. M. (1995). Does saccadic undershoot minimize saccadic flight-time? A Monte-Carlo study. *Vision Research*, 35, 691–701.
- Harvey, B. M., & Dumoulin, S. O. (2011). The relationship between cortical magnification factor and population receptive field size in human visual cortex: Constancies in cortical architecture. *Journal of Neuroscience*, 31, 13604–13612.
- Henson, D. (1978). Corrective saccades: Effects of altering visual feedback. *Vision Research*, 18, 63–67.
- Hubel, D. H., & Wiesel, T. N. (1974). Uniformity of monkey striate cortex: A parallel relationship between field size, scatter, and magnification factor. *Journal of Comparative Neurology*, 158, 295–306.
- Infante, C., & Leiva, J. (1986). Simultaneous unitary neuronal activity in both superior colliculi and its relation to eye movements in the cat. *Brain Research*, 381, 390–392.
- Isa, T., & Hall, W. C. (2009). Exploring the superior colliculus in vitro. *Journal of Neurophysiology*, 102, 2581–2593.
- Kalesnykas, R. P., & Hallett, P. E. (1994). Retinal eccentricity and the latency of eye saccades. *Vision Research*, 34, 517–531.
- Kapoula, Z. (1985). Evidence for a range effect in the saccadic system. *Vision Research*, 25, 1155–1157.
- Lee, C., Rohrer, W. H., & Sparks, D. L. (1988).

- Population coding of saccadic eye movements by neurons in the superior colliculus. *Nature*, 332, 357–360.
- Lemij, H. G., & Collewijn, H. (1989). Differences in accuracy of human saccades between stationary and jumping targets. *Vision Research*, 29, 1737–1748.
- Marino, R. A., Rodgers, C. K., Levy, R., & Munoz, D. P. (2008). *Journal of Neurophysiology* 100, 2564–2576.
- McIlwain, J. T. (1975). Visual receptive fields and their images in superior colliculus of the cat. *Journal of Neurophysiology*, 38, 219–230.
- McIlwain, J. T. (1982). Lateral spread of neural excitation during microstimulation in intermediate gray layer of cat's superior colliculus. *Journal of Neurophysiology*, 47, 167–178.
- McIlwain, J. T. (1986). Point images in the visual system: New interest in an old idea. *Trends in Neuroscience*, 9, 354–358.
- McIlwain, J. T. (1991). Distributed spatial coding in the superior colliculus: A review. *Visual Neuroscience*, 6, 3–13.
- Meredith, M. A., & Ramoa, A. S. (1998). Intrinsic circuitry of the superior colliculus: Pharmacophysiological identification of horizontally oriented inhibitory interneurons. *Journal of Neurophysiology*, 79, 1597–1602.
- Moschovakis, A. K., Gregoriou, G. G., & Savaki, H. E. (2001). Functional imaging of the primate superior colliculus during saccades to visual targets. *Nature Neuroscience*, 4, 1026–1031.
- Munoz, D. P., & Istvan, P. J. (1998). Lateral inhibitory interactions in the intermediate layers of the monkey superior colliculus. *Journal of Neurophysiology*, 79, 1193–1209.
- Munoz, D. P., & Wurtz, R. H. (1995a). Saccade-related activity in monkey superior colliculus: I. Characteristics of burst and buildup cells. *Journal of Neurophysiology*, 73, 2313–2333.
- Munoz, D. P., & Wurtz, R. H. (1995b). Saccade-related activity in monkey superior colliculus: II. Spread of activity during saccades. *Journal of Neurophysiology*, 73, 2334–2348.
- Nakahara, H., Morita, K., & Wurtz, R. H., Optican, L. M. (2006). Saccade-related spread of activity across superior colliculus may arise from asymmetry of internal connections. *Journal of Neurophysiology*, 96, 765–774.
- Nuthmann A., Vitu, F., Engbert, R., & Kliegl, R. (2016). No evidence for a saccadic range effect for visually guided and memory guided saccades in simple saccade-targeting tasks. *PLoS One*, 11, e0162449.
- Olivier, E., Corvisier, J., Pauluis, Q., & Hardy, O. (2000). Evidence for glutamatergic tectotectal neurons in the cat superior colliculus: a comparison with GABAergic tectotectal neurons. *European Journal of Neuroscience*, 12, 2354–2366.
- Olivier, E., Porter, J. D., & May, P. J. (1998). Comparison of the distribution and somatodendritic morphology of tectotectal neurons in the cat and monkey. *Visual Neuroscience*, 15, 903–922.
- Ottes, F. P., van Gisbergen, J. A., & Eggermont, J. J. (1986). Visuomotor fields of the superior colliculus: a quantitative model. *Vision Research*, 26, 857–873.
- Paré, M., & Guitton, D. (1994). The fixation area of the cat superior colliculus: Effects of electrical stimulation and direct connection with brainstem omnipause neurons. *Experimental Brain Research*, 101, 109–122.
- Péllisson, D., Alahyane, N., Panouillères, M., & Tilikete, C. (2010). Sensorimotor adaptation of saccadic eye movements. *Neuroscience & Biobehavioral Reviews*, 34, 1103–1120.
- Phongphanphane, P., Marino, R. A., Kaneda, K., Yanagawa, Y., Munoz, D. P., & Isa, T. (2014). Distinct local circuit properties of the superficial and intermediate layers of the rodent superior colliculus. *European Journal of Neuroscience*, 40, 2329–2343.
- Pinheiro, J. C., & Bates, D. M. (1996). Unconstrained parametrizations for variance-covariance matrices. *Statistics and Computing*, 6, 289–296.
- Polyak, S. (1957). *The vertebrate visual system*. Chicago, IL: University of Chicago Press.
- R Core Team. (2012). *R: A language and environment for statistical computing*. Vienna, Austria: R Foundation for Statistical Computing ISBN. <http://www.R-project.org/>.
- Robinson, D. A. (1972). Eye movements evoked by collicular stimulation in the alert monkey. *Vision Research*, 12, 1795–1808.
- Robinson, D. A. (1973). Models of the saccadic eye movement control system. *Kybernetik*, 14, 71–83.
- Rovamo, J., Virsu, V., Nasanen, R. (1978). Cortical magnification factor predicts photopic contrast sensitivity of peripheral vision. *Nature*, 271, 54–56.
- Schiller, P. H., & Stryker, M. (1972). Single-unit recording and stimulation in superior colliculus of the alert rhesus monkey. *Journal of Neurophysiology*, 35, 915–924.
- Schwartz, E. L. (1980). Computational anatomy and functional architecture of striate cortex: A spatial

- mapping approach to perceptual coding. *Vision Research*, 20, 645–669.
- Sparks, D. L., Holland, R., & Guthrie, B. L. (1976). Size and distribution of movement fields in the monkey superior colliculus. *Brain Research*, 113, 21–34.
- Sommer, M. A., & Wurtz, R. H. (2000). Composition and topographic organization of signals sent from the frontal eye field to the superior colliculus. *Journal of Neurophysiology*, 83, 1979–2001.
- Takahashi, M., Sugiuchi, Y., Izawa, Y., & Shinoda, Y. (2005). Commissural excitation and inhibition by the superior colliculus in tectoreticular neurons projecting to omnipause neuron and inhibitory burst neuron regions. *Journal of Neurophysiology*, 94, 1707–1726.
- Takeichi, N., Kaneko, C. R., & Fuchs, A. F. (2007). Activity changes in monkey superior colliculus during saccade adaptation. *Journal of Neurophysiology*, 97, 4096–4107.
- van Essen, D. C., Newsome, W. T., & Maunsell, J. H. R. (1984). The visual field representation in striate cortex of the macaque monkey: Asymmetries, anisotropies, and individual variability. *Vision Research*, 24, 429–448.
- van Opstal, A. J., & van Gisbergen, J. A. (1989a). A model for collicular efferent mechanisms underlying the generation of saccades. *Biological Cybernetics*, 60, 171–183.
- van Opstal, A. J., & van Gisbergen, J. A. (1989b). Scatter in the metrics of saccades and properties of the collicular motor map. *Vision Research*, 29, 1183–1196.
- van Opstal, A. J., van Gisbergen, J. A., & Smith, A. C. (1990). Comparison of saccades evoked by visual stimulation and collicular electrical stimulation in the alert monkey. *Experimental Brain Research*, 79, 299–312.
- van Rensbergen, J., & de Troy, A. (1993). *A reference guide for the Leuven dual-pc controlled purkinge eyetracking system* [Technical report]. Laboratory of Experimental Psychology, Catholic University of Leuven.
- Vitu, F. (1991). The existence of a center of gravity effect during reading. *Vision Research*, 31, 1289–1313.
- Vitu, F., Lancelin, D., Jean, A., & Farioli, F. (2006). Influence of foveal distractors on saccadic eye movements: A dead zone for the global effect. *Vision Research*, 46, 4684–4708.
- White, B. J., & Munoz, D. P. (2011). The superior colliculus. In S. P. Liversedge, I. D. Gilchrist, & S. Everling (Eds.), *Oxford handbook on eye movements* (pp. 195–213). Oxford, UK: Oxford University Press.
- Wurtz, R. H., & Goldberg, M. E. (1972). Activity of superior colliculus in behaving monkey. III. Cells discharging before eye movements. *Journal of Neurophysiology*, 35, 575–586.
- Zuur, A., Ieno, E. N., Walker, N., Saveliev, A. A., & Smith, G. M. (2009). *Mixed effects models and extensions in ecology with R*. New York: Springer.

Appendix 1

In Tables A1–A9 below, the fixed effects of optimal LME models (with the optimal random structure in the legend) are reported for the different dependent variables in HM-VM and HM data sets. The intercept estimate gives the value of the dependent variable when all variables were at their reference value (HM-VM: eccentricity = 6.42° and direction = 0°; HM1-3: eccentricity = 3.11°, 6.96°, and 7.97°, respectively). Other estimates correspond to regression coefficients. Colon stands for interaction. In Table A10, the fixed effects of optimal LME models (with the optimal random structure in the legend) are reported for only two dependent variables in HM-VM and HM data sets but with latency bin (with two levels, 1 and 2; see Results section) and its interaction with the other factors as additional predictors. As latency bin was entered as a categorical predictor, the reference level was 1; it is referred to as bin in Table A10.

Fixed effects/DV = area (sq. degrees vs. sq. mm)

	A. Visual space					B. SC space				
	Estimate	SE	df	t value	p value	Estimate	SE	df	t value	p value
HM-VM										
(Intercept)	2.96007	0.23443	412	12.627	0.0000	0.06982	0.01887	409	3.699	0.0002
Eccentricity	0.35627	0.04842	412	7.358	0.0000	-0.00209	0.00222	409	-0.940	0.3476
Direction						0.00098	0.00020	409	4.927	0.0000
Eccentricity ²						0.00144	0.00046	409	3.124	0.0019
Eccentricity:direction						-0.00013	0.00004	409	-3.518	0.0005
HM1										
(Intercept)	1.23495	0.12552	78	9.839	0.0000	0.07941	0.00723	78	10.975	0.0000
Eccentricity	0.21068	0.04327	78	4.869	0.0000	-0.01739	0.00324	78	-5.370	0.0000
Eccentricity ²	0.03658	0.01326	78	2.758	0.0072	0.00570	0.00169	78	3.376	0.0011
HM2										
(Intercept)	1.93022	0.23410	94	8.245	0.0000	0.04880	0.00800	94	6.096	0.0000
Eccentricity	0.27424	0.03824	94	7.172	0.0000	-0.00460	0.00101	94	-4.559	0.0000
Eccentricity ²	0.01752	0.00623	94	2.810	0.0060	0.00111	0.00021	94	5.326	0.0000
HM3										
(Intercept)	1.82599	0.17603	110	10.373	0.0000	0.03480	0.00689	110	5.051	0.0000
Eccentricity	0.24151	0.01921	110	12.571	0.0000	-0.00537	0.00147	110	-3.659	0.0004
Eccentricity ²	0.02489	0.00506	110	4.919	0.0000	0.00131	0.00018	110	7.103	0.0000

Table A1. Area subtended by 90% isolines (A: in squared degrees of visual angle; B: in squared millimeters of SC space). *Notes:* In visual space (A), the optimal random structure (by participants) included a random intercept and random effects of eccentricity and direction in HM-VM, both a random intercept and a random effect of eccentricity in HM1 and HM2, and only a random intercept in HM3. In SC space (B), the optimal random structure (by participants) included both a random intercept and a random effect of direction in HM-VM, a random intercept and random linear and quadratic effects of eccentricity in HM1 and HM3, and a random intercept and a random effect of eccentricity in HM2.

Fixed effects/DV = major-axis length (degrees vs. mm)

	A. Visual space					B. SC space				
	Estimate	SE	df	t value	p value	Estimate	SE	df	t value	p value
HM-VM										
(Intercept)	2.20039	0.11639	412	18.905	0.0000	0.29367	0.03524	409	8.333	0.0000
Eccentricity	0.17250	0.02413	412	7.150	0.0000	-0.00436	0.00524	409	-0.831	0.4064
Direction						0.00230	0.00034	409	6.849	0.0000
Eccentricity ²						0.00301	0.00078	409	3.868	0.0001
Eccentricity:direction						-0.00027	0.00006	409	-4.210	0.0000
HM1										
(Intercept)	1.37980	0.07607	79	18.138	0.0000	0.33320	0.01882	78	17.699	0.0000
Eccentricity	0.11582	0.02004	79	5.780	0.0000	-0.03666	0.00498	78	-7.361	0.0000
Eccentricity ²						0.01029	0.00209	78	4.912	0.0000
HM2										
(Intercept)	1.67687	0.11226	94	14.937	0.0000	0.25163	0.01814	94	13.869	0.0000
Eccentricity	0.13477	0.01624	94	8.299	0.0000	-0.01037	0.00234	94	-4.429	0.0000
Eccentricity ²	0.00642	0.00282	94	2.277	0.0251	0.00247	0.00045	94	5.457	0.0000
HM3										
(Intercept)	1.64129	0.09068	110	18.099	0.0000	0.21884	0.00678	110	16.129	0.0000
Eccentricity	0.11702	0.00804	110	14.549	0.0000	-0.01137	0.00251	110	-4.532	0.0000
Eccentricity ²	0.00928	0.00212	110	4.379	0.0000	0.00274	0.00033	110	8.256	0.0000

Table A2. Length of the major axis of the ellipse fitted to the 90% isoline area (A: in degrees of visual angle; B: in millimeters of SC space). *Notes:* In visual space (A), the optimal random structure (by participants) included a random intercept and random effects of eccentricity and direction in HM-VM, both a random intercept and a random effect of eccentricity in HM1 and HM2, and only a random intercept in HM3. In SC space (B), the optimal random structure (by participants) included both a random intercept and random effects of eccentricity and direction in HM-VM and a random intercept and a random effect of eccentricity in HM data sets.

Fixed effects/DV = minor-axis length (degrees vs. mm)

	A. Visual space					B. SC space				
	Estimate	SE	df	t value	p value	Estimate	SE	df	t value	p value
HM-VM										
(Intercept)	1.60067	0.04606	412	34.751	0.0000	0.29275	0.02985	410	9.806	0.0000
Eccentricity	0.08236	0.00919	412	8.957	0.0000	-0.00937	0.00138	410	-6.781	0.0000
Direction						0.00099	0.00037	410	2.648	0.0084
Eccentricity ²						0.00125	0.00054	410	2.297	0.0221
HM1										
(Intercept)	1.14961	0.04367	78	26.327	0.0000	0.29773	0.01185	78	25.114	0.0000
Eccentricity	0.08594	0.00943	78	9.114	0.0000	-0.02450	0.00440	78	-5.569	0.0000
Eccentricity ²	0.01158	0.00581	78	1.994	0.0496	0.00745	0.00241	78	3.094	0.0027
HM2										
(Intercept)	1.43467	0.05286	95	27.141	0.0000	0.23751	0.01433	94	16.570	0.0000
Eccentricity	0.07912	0.00797	95	9.928	0.0000	-0.00888	0.00176	94	-5.054	0.0000
Eccentricity ²						0.00201	0.00035	94	5.735	0.0000
HM3										
(Intercept)	1.38132	0.04715	110	29.298	0.0000	0.20998	0.01009	110	20.799	0.0000
Eccentricity	0.06776	0.00961	110	7.052	0.0000	-0.00970	0.00189	110	-5.142	0.0000
Eccentricity ²	0.00493	0.00126	110	3.917	0.0002	0.00229	0.00027	110	8.612	0.0000

Table A3. Length of the minor axis of the ellipse fitted to the 90% isoline area (A: in degrees of visual angle; B: in millimeters of SC space). *Notes:* In visual space (A), the optimal random structure (by participants) included a random intercept and random effects of eccentricity and direction in HM-VM, both a random intercept and a random effect of eccentricity in HM2 and HM3, and only a random intercept in HM1. In SC space (B), the optimal random structure (by participants) included both a random intercept and a random effect of direction in HM-VM, a random intercept and random linear and quadratic effects of eccentricity in HM1, and both a random intercept and a random effect of eccentricity in HM2 and HM3.

Fixed effects/DV = major-to-minor-axis ratio

	A. Visual space					B. SC space				
	Estimate	SE	df	t value	p value	Estimate	SE	df	t value	p value
HM-VM										
(Intercept)	0.22576	0.04136	411	5.458	0.0000	0.02673	0.01537	409	1.739	0.0828
Eccentricity	0.03677	0.00832	411	4.420	0.0000	0.00453	0.00740	409	0.612	0.5406
Direction	0.00194	0.00031	411	6.232	0.0000	0.00315	0.00045	409	6.984	0.0000
Eccentricity ²						0.00352	0.00095	409	3.712	0.0002
Eccentricity:direction						-0.00043	0.00008	409	-5.522	0.0000
HM1										
(Intercept)	0.13581	0.02092	80	6.491	0.0000	0.11462	0.02167	78	5.289	0.0000
Eccentricity						-0.02792	0.00514	78	-5.427	0.0000
Eccentricity ²						0.00482	0.00175	78	2.755	0.0073
HM2										
(Intercept)	0.18372	0.03033	95	6.057	0.0000	0.05204	0.00938	95	5.549	0.0000
Eccentricity	0.02575	0.00582	95	4.424	0.0000					
Eccentricity ²						0.00117	0.00058	95	2.004	0.0479
HM3										
(Intercept)	0.20007	0.02832	111	7.064	0.0000	0.04403	0.00813	110	5.413	0.0000
Eccentricity	0.02037	0.00404	111	5.036	0.0000	-0.00286	0.00118	110	-2.420	0.0172
Eccentricity ²						0.00081	0.00038	110	2.121	0.0362

Table A4. Ratio of major-to-minor-axis lengths of the fitted ellipses. *Notes:* One was subtracted from the obtained ratio to test whether the ratio differed significantly from 1 (intercept estimate). In visual space (A), the optimal random structure (by participants) included a random intercept and random linear and quadratic effects of eccentricity in HM-VM, HM2, and HM3 and both a random intercept and a random effect of eccentricity in HM1. In SC space (B), the optimal random structure (by participants) included a random intercept and random effects of eccentricity and direction in HM-VM, a random intercept and random linear and quadratic effects of eccentricity in HM2 and HM3, and both a random intercept and a random effect of eccentricity in HM1.

Fixed effects/DV = asymmetry (in degrees vs. mm)

	A. Visual space					B. SC space				
	Estimate	SE	df	t value	p value	Estimate	SE	df	t value	p value
HM-VM										
(Intercept)	0.14266	0.02262	412	6.307	0.0000	0.00961	0.00438	410	2.196	0.0287
Eccentricity	0.02207	0.00431	412	5.124	0.0000	0.00067	0.00105	410	0.644	0.5198
Direction						0.00031	0.00013	410	2.463	0.0142
Eccentricity:direction						−0.00004	0.00001	410	−2.999	0.0029
HM1										
(Intercept)	0.02853	0.00648	79	4.405	0.0000	0.00947	0.00129		7.366	0.0000
Eccentricity						−0.00171	0.00055		−3.097	0.0026
Eccentricity ²	0.00389	0.00128	79	3.025	0.0033	0.00068	0.00034		2.008	0.0478
HM2										
(Intercept)	0.07707	0.01121	95	6.877	0.0000	0.01038	0.00099		10.460	0.0000
Eccentricity	0.00986	0.00188	95	5.248	0.0000					
HM3										
(Intercept)	0.05761	0.00846	111	6.807	0.0000	0.00735	0.00102	112	7.213	0.0000
Eccentricity	0.01235	0.00324	111	3.809	0.0004					

Table A5. Asymmetry of landing-position distributions (A: in degrees of visual angle; B: in millimeters of SC space). *Notes:* In visual space (A), the optimal random structure (by participants) included a random intercept and random effects of eccentricity and direction in HM-VM, both a random intercept and a random effect of eccentricity in HM1, a random intercept in HM2, and a random intercept and random linear and quadratic effects of eccentricity in HM3. In SC space (B), the optimal random structure (by participants) included a random intercept and random effects of eccentricity and direction in HM-VM, a random intercept and a random quadratic effect of eccentricity in HM3, and no random component in HM1 and HM2.

Fixed effects/DV = amplitude skewness (in degrees vs. mm)

	A. Visual space					B. SC space				
	Estimate	SE	df	t value	p value	Estimate	SE	df	t value	p value
HM-VM										
(Intercept)	−0.04732	0.02054	412	−2.303	0.0218	−0.00609	0.00247	410	−2.466	0.0141
Eccentricity						0.00033	0.00086	410	0.382	0.7027
Direction	0.00121	0.00045	412	2.678	0.0077	0.00002	0.00006	410	0.376	0.7071
Eccentricity:direction						−0.00004	0.00001	410	−2.624	0.0090
HM1										
(Intercept)	0.00121	0.00675		0.179	0.8582	−0.00209	0.00125	80	−1.678	0.0972
Eccentricity	−0.00835	0.00410		−2.038	0.0446					
HM2										
(Intercept)	−0.02996	0.00991		−3.023	0.0032	−0.00274	0.00130		−2.099	0.0383
Eccentricity	−0.00573	0.00266		−2.151	0.0338					
HM3										
(Intercept)	−0.04201	0.01013		−4.148	0.0001	−0.00582	0.00161	110	−3.623	0.0004
Eccentricity	−0.01198	0.00235		−5.088	0.0000	−0.00129	0.00065	110	−1.992	0.0488
Eccentricity ²						0.00013	0.00006	110	2.005	0.0475

Table A6. Skewness of landing-position distributions along the eccentricity (amplitude)/u-axis (A: in degrees of visual angle; B: in millimeters of SC space). *Notes:* In visual space (A), the optimal random structure (by participants) included a random intercept and random effects of eccentricity and direction in HM-VM but no random component in HM data sets. In SC space (B), the optimal random structure (by participants) included a random intercept and a random effect of direction in HM-VM, a random intercept and a random quadratic effect of eccentricity in HM1, a random intercept and a random linear effect of eccentricity in HM3, and no random component in HM2.

Fixed effects/DV = direction skewness (in degrees vs. mm)

	A. Visual space					B. SC space				
	Estimate	SE	df	t value	p value	Estimate	SE	df	t value	p value
HM-VM										
(Intercept)	0.00046	0.00626	413	0.073	0.9415	0.00253	0.00114		2.226	0.0265
Direction						-0.00007	0.00002		-3.752	0.0002
HM1										
(Intercept)	0.00311	0.00311	80	1.000	0.3203	0.00129	0.00080		1.599	0.1133
HM2										
(Intercept)	-0.00226	0.00650	94	-0.348	0.7287	-0.00004	0.00050		-0.083	0.9340
Eccentricity	-0.00315	0.00131	94	-2.410	0.0179	-0.00033	0.00013		-2.449	0.0160
Eccentricity ²	-0.00046	0.00025	94	-1.799	0.0753					
HM3										
(Intercept)	0.00269	0.00407	112	0.661	0.5098	-0.00048	0.00053		-0.899	0.3705

Table A7. Skewness of landing-position distributions along the direction/*v*-axis (A: in degrees of visual angle; B: in millimeters of SC space). *Notes:* In visual space (A), the optimal random structure (by participants) included a random intercept and random effects of eccentricity and direction in HM-VM and a random intercept and random linear and quadratic effects of eccentricity in HM data sets. In SC space (B), none of the models had a random component.

Fixed effects/DV = amplitude error (in degrees vs. mm)

	A. Visual space					B. SC space				
	Estimate	SE	df	t value	p value	Estimate	SE	df	t value	p value
HM-VM										
(Intercept)	-0.37435	0.03818	410	-9.803	0.0000	-0.04887	0.00549	410	-8.907	0.0000
Eccentricity	-0.05723	0.01874	410	-3.054	0.0024	-0.00270	0.00352	410	-0.769	0.4425
Direction	-0.00060	0.00212	410	-0.282	0.7779	0.00010	0.00027	410	0.375	0.7076
Eccentricity:direction	-0.00052	0.00016	410	-3.247	0.0013	-0.00007	0.00003	410	-2.887	0.0041
HM1										
(Intercept)	-0.13969	0.03794	79	-3.681	0.0004	-0.02994	0.00938	80	-3.193	0.0020
Eccentricity	-0.02976	0.01278	79	-2.329	0.0224					
HM2										
(Intercept)	-0.20700	0.05052	95	-4.098	0.0001	-0.03119	0.00718	96	-4.342	0.0000
Eccentricity	-0.02576	0.00946	95	-2.723	0.0077					
HM3										
(Intercept)	-0.12930	0.05659	110	-2.284	0.0242	-0.0280	0.00701	112	-4.000	0.0001
Eccentricity	-0.02582	0.00562	110	-4.597	0.0000					
Eccentricity ²	-0.00174	0.00088	110	-1.973	0.0510					

Table A8. Landing-position error along the eccentricity (amplitude)/*u*-axis (A: radial error in degrees of visual angle, B: *u*-error in millimeters of SC space). *Notes:* In visual space (A), the optimal random structure (by participants) included a random intercept, random linear and quadratic effects of eccentricity and a random effect of direction in HM-VM, both a random intercept and a random effect of eccentricity in HM1 and HM3, and a random intercept and random linear and quadratic effects of eccentricity in HM2. In SC space (B), the optimal random structure (by participants) included a random intercept, random linear and quadratic effects of eccentricity and a random effect of direction in HM-VM, a random intercept and a random effect of eccentricity in HM1 and HM2, and a random intercept and random linear and quadratic effects of eccentricity in HM3.

Fixed effects/DV = saccade latency (in ms)					
	Estimate	SE	df	t value	p value
HM-VM					
(Intercept)	172.0223	7.85116	8977	21.910	0.0000
Eccentricity ²	0.40547	0.03761	8977	10.781	0.0000
Direction	-0.10933	0.05493	8977	-1.990	0.0466
HM1					
(Intercept)	183.3785	4.44515	2873	41.254	0.0001
Eccentricity	-5.50019	1.26583	2873	-4.345	0.0001
Eccentricity ²	3.65447	0.66412	2873	5.503	0.0001
HM2					
(Intercept)	164.3329	7.13620	3458	23.028	0.0001
Eccentricity ²	0.68027	0.18089	3458	3.761	0.0002
HM3					
(Intercept)	166.8779	8.48744	3939	19.662	0.0000
Eccentricity	-0.68506	0.40753	3939	-1.681	0.0928
Eccentricity ²	0.53558	0.07319	3939	7.317	0.0000

Table A9. Saccade latency. *Notes:* The optimal random structure (by participants) included a random intercept and random effects of target eccentricity and direction in HM-VM and a random intercept as well as random linear and quadratic effects of target eccentricity in HM data sets.

Latency-based analyses in visual space/fixed effects for different dependent variables

	A. Area (sq. degrees)					B. Amplitude error (degrees)				
	Estimate	SE	df	t value	p value	Estimate	SE	df	t value	p value
HM-VM										
(Intercept)	2.45421	0.15705	748	15.626	0.000	−0.43863	0.05306	745	−8.266	0.0000
Eccentricity	0.24644	0.03058	748	8.058	0.000	−0.08263	0.02354	745	−3.510	0.0005
Direction						−0.00077	0.00192	745	−0.404	0.6864
Bin2	−0.20875	0.07855	748	−2.657	0.008	0.06601	0.04531	745	1.457	0.1456
Eccentricity:direction						−0.00043	0.00016	745	−2.759	0.0059
Eccentricity:bin2						0.03972	0.00957	745	4.148	0.0000
HM1										
(Intercept)	1.34129	0.12691	166	10.568	0.0000	−0.22544	0.04704	163	−4.792	0.0000
Eccentricity	0.19598	0.04826	166	4.060	0.0001	−0.07239	0.01429	163	−5.067	0.0000
Eccentricity ²						0.00765	0.00361	163	2.117	0.0358
Bin2	−0.26368	0.07723	166	−3.414	0.0008	0.16331	0.05732	163	2.849	0.0050
Eccentricity:bin2						0.07761	0.00835	163	9.296	0.0000
Eccentricity ² :bin2						−0.01295	0.00514	163	−2.519	0.0127
HM2										
(Intercept)	1.81584	0.21666	196	8.381	0.0000	−0.27560	0.05948	197	−4.633	0.0000
Eccentricity	0.26493	0.03464	196	7.648	0.0000	−0.05398	0.00957	197	−5.641	0.0000
Eccentricity ²	0.01319	0.00659	196	2.003	0.0466					
Bin2	−0.39303	0.09611	196	−4.089	0.0001	0.12979	0.03493	197	3.716	0.0003
Eccentricity:bin2	−0.08784	0.02582	196	−3.402	0.0008	0.05339	0.00631	197	8.454	0.0000
HM3										
(Intercept)	2.00802	0.13869	228	14.478	0.0000	−0.21408	0.06259	229	−3.420	0.0007
Eccentricity	0.22348	0.01964	228	11.378	0.0000	−0.05027	0.00708	229	−7.099	0.0000
Eccentricity ²	0.01667	0.00545	228	3.061	0.0025					
Bin2	−0.69938	0.11545	228	−6.058	0.0000	0.14410	0.04091	229	3.523	0.0005
Eccentricity:bin2	−0.05543	0.02684	228	−2.065	0.0401	0.04541	0.00521	229	8.709	0.0000

Table A10. Latency-based analyses of the area subtended by 90% isolines (A) and the radial landing-position error (B) in visual space. *Notes:* For the area, the optimal random structure (by participants) included a random intercept and random effects of eccentricity and direction in HM-VM, a random intercept and a random linear effect of eccentricity in HM1, and a random intercept and random linear and quadratic effects of eccentricity in HM2 and HM3. For the landing-position error, the optimal random structure (by participants) included a random intercept, random linear and quadratic effects of eccentricity, and random effects of direction and latency bin in HM-VM; a random intercept and random effects of eccentricity and latency bin in HM1; a random intercept, random linear and quadratic effects of eccentricity, and a random effect of latency bin in HM2; and a random intercept and a random quadratic effect of eccentricity in HM3.